nature biotechnology

ARTICLES

https://doi.org/10.1038/s41587-019-0197-9

Epicardial cells derived from human embryonic stem cells augment cardiomyocyte-driven heart regeneration

Johannes Bargehr[1,2], Lay Ping Ong[1,2], Maria Colzani[1,2], Hongorzul Davaapil[1,2], Peter Hofsteen[3], Shiv Bhandari[3], Laure Gambardella[1,2], Nicolas Le Novère[4], Dharini Iyer[1,2], Fotios Sampaziotis[1], Florian Weinberger[3], Alessandro Bertero[3], Andrea Leonard[3], William G. Bernard[1,2], Amy Martinson[3], Nichola Figg[2], Michael Regnier[5], Martin R. Bennett[2], Charles E. Murry[3,5,6,7*] and Sanjay Sinha[1,2,7*]

The epicardium and its derivatives provide trophic and structural support for the developing and adult heart. Here we tested the ability of human embryonic stem cell (hESC)-derived epicardium to augment the structure and function of engineered heart tissue in vitro and to improve efficacy of hESC-cardiomyocyte grafts in infarcted athymic rat hearts. Epicardial cells markedly enhanced the contractility, myofibril structure and calcium handling of human engineered heart tissues, while reducing passive stiffness compared with mesenchymal stromal cells. Transplanted epicardial cells formed persistent fibroblast grafts in infarcted hearts. Cotransplantation of hESC-derived epicardial cells and cardiomyocytes doubled graft cardiomyocyte proliferation rates in vivo, resulting in 2.6-fold greater cardiac graft size and simultaneously augmenting graft and host vascularization. Notably, cotransplantation improved systolic function compared with hearts receiving either cardiomyocytes alone, epicardial cells alone or vehicle. The ability of epicardial cells to enhance cardiac graft size and function makes them a promising adjuvant therapeutic for cardiac repair.

Despite major advances in the treatment of heart failure due to systolic impairment, therapeutic approaches have fallen short of addressing the cause of the problem; injury of the mammalian heart leads to irreversible loss of contractile myocardial tissue which is incapable of regeneration. At the turn of the millennium heart failure was widely identified as an emerging epidemic[1]. To date, 5.6 million patients in the United States alone and 23 million worldwide are suffering from heart failure, with 50% dying within 5 yr after being diagnosed[2,3]. Current treatment is limited to ameliorating symptoms and slowing the natural progression of the disease but fails to compensate for the loss of contractile myocardium postinjury.

Regenerative medicine may hold the key to effectively treating heart failure by using stem-cell-derived cardiovascular cells and tissues to restore full contractile function[4,5]. Of all stem cell types, human pluripotent stem cells such as hESCs and induced pluripotent stem cells have the greatest potential for forming cardiovascular tissues, reliably giving rise to cardiomyocytes (CMs)[6–8], endothelial cells[9,10], smooth muscle cells[11] and more recently epicardial and endocardial-like cells[12–15] under chemically defined conditions. Furthermore, hESC-derived CMs have been successfully used to remuscularize infarcted rat[8] and guinea pig[16,17] hearts, resulting in electrical integration and preserving cardiac function. The clinical potential of this technology has also been demonstrated in non-human primate models, where transplantation of human or monkey pluripotent stem cell-derived CMs resulted in substantial remuscularization of the infarcted heart and restoration of cardiac function[18–20].

While mammalian heart regeneration has made progress, hurdles remain, such as relative immaturity of transplanted cells, suboptimal graft retention, insufficient cellular proliferation and a small graft size. In vitro, human pluripotent stem cell (hPSC)-derived CMs derived from most protocols at best resemble CMs found in a first trimester fetus, which may limit the functional benefits post-transplantation[21]. To date, little attention has been devoted to a supportive cell type that would promote maturity of hESC-derived CMs and increase the graft size post-transplantation in vivo.

In early mammalian heart development, the epicardium plays a pivotal role as a progenitor cell source and provides trophic support for developing CMs. Because the epicardium gives rise to cardiac fibroblasts and coronary smooth muscle cells, it is essential for the formation of a functioning connective tissue and coronary vasculature[22,23]. Moreover, epicardium-derived cells (EPDCs) are essential for cardiac proliferation and compaction[24–26] and have been reported to promote CM maturation[27–29]. Given their trophic role in heart development, we hypothesized that epicardial cells could promote CM maturation and contractility in hESC-based three-dimensional (3D)-EHTs in vitro and enhance engraftment and maturity leading to potential functional benefits when cotransplanted with hESC-derived CMs in vivo.

[1]The Anne McLaren Laboratory, Wellcome Trust – MRC Cambridge Stem Cell Institute, University of Cambridge, Cambridge, UK. [2]Division of Cardiovascular Medicine, University of Cambridge, Cambridge, UK. [3]Department of Pathology, Center for Cardiovascular Biology, Institute for Stem Cell and Regenerative Medicine, University of Washington, Seattle, WA, USA. [4]The Babraham Institute, Cambridge, UK. [5]Department of Bioengineering, University of Washington, Seattle, WA, USA. [6]Division of Cardiology, Department of Medicine, University of Washington, Seattle, WA, USA. [7]These authors contributed equally: Charles E. Murry, Sanjay Sinha. *e-mail: murry@uw.edu; ss661@cam.ac.uk

We report here that hESC-derived epicardium promotes the development of three-dimensional engineered heart tissues (3D-EHTs) in vitro and cardiac grafts in vivo via CM maturation, proliferation and contraction. In the infarcted heart, hESC-derived epicardial cells (hESC-EPIs) also increase endogenous neo-vessel development and enhance hESC-CM proliferation and subsequent maturation, thus creating larger grafts of human myocardium that further enhance ventricular function. By recapitulating key developmental steps, the epicardium augmented CM function, making it a promising adjuvant therapy in regenerative medicine.

Results

hESC-EPIs promote CM maturation in 3D-EHTs. We first generated hESC-derived green fluorescent protein (GFP)-transgenic epicardial cells and wild-type (WT) CMs as previously described[8,12] (Fig. 1a,b). Epicardial cells expressed epicardial and epithelial markers, WT1 and pan-cytokeratin, but no mesenchymal markers such as vimentin after their derivation in vitro[12,30]. The functionality of epicardial cells was initially demonstrated through differentiating them to cardiac fibroblasts in vitro under chemically defined conditions that included VEGF and FGF. At the end of this differentiation protocol they expressed the fibroblast and mesenchymal markers, S100A4, DDR2 and vimentin, but lost their epithelial character indicating successful epithelial-to-mesenchymal transition (EMT). During epicardial to fibroblast differentiation, WT1 was downregulated while the fibroblast marker S100A4 was gradually upregulated. (Supplementary Fig. 1a–e).

Next, we tested the utility of epicardial cells in the context of 3D-EHTs. We incorporated epicardial cells along with hESC-CMs into collagen-based 3D-EHTs[31], which developed for 14 d under passive stress before they were subjected to histological and functional assessment (Fig. 1c,d). To investigate the potency of epicardial cells in 3D-EHTs, we compared them with constructs containing: (1) CMs alone; (2) CMs and hESC-derived mesenchymal cells; and (3) CMs and primary human mesenchymal stromal cells (MSCs) from bone marrow. Epicardial cells as well as primary mesenchymal cells had the strongest effects on tissue remodeling and compaction, whereas tissues containing high-purity CMs alone demonstrated minimal compaction (Fig. 1e–g).

Whilst in the tissues, hESC-EPIs underwent EMT as indicated by the increase in expression of vimentin and decrease in pan-cytokeratin, comparing constructs after 7 d and 14 d of development. In this context, epicardial derivates have previously been termed EPDCs[23]. EPDCs are positive for vimentin and S100A4, indicative of a fibroblast phenotype (Supplementary Fig. 2a–c).

To determine the state of CM maturity, histological sections of the 3D-EHTs were stained for sarcomeric proteins, and the sarcomere length, cell diameter, cell sectional area and myofibril alignment were quantified. HESC-EPIs promoted the greatest sarcomere length, cell diameter, cell sectional area and myofibril alignment, which correlate with CM maturation, compared with primary MSCs, hESC-derived MSCs or CM alone (Fig. 1h–j and Supplementary Fig. 3a). 3D-EHTs containing hESC-EPIs and primary MSCs exhibited the greatest degree of sarcomeric organization (Supplementary Fig. 3b). Furthermore, constructs containing hESC-EPIs expressed more connexin 43, a marker of electrical connectivity between CMs, compared with the other groups (Supplementary Fig. 2d, e). Gene expression by quantitative PCR with reverse transcription (RT–qPCR) demonstrated trends consistent with increases in the ratios of adult/fetal isoforms of contractile proteins (*MYH7/MYH6*, *MYL2/MYL7* and *TNNI3/TNNI1)*, all indicators of CM maturity (Supplementary Fig. 4). In conclusion, hESC-EPIs replicate key steps of early embryonic heart development in 3D-EHTs, resulting in increased CM maturation.

hESC-EPIs enhance functional maturation of 3D-EHT. We next tested whether the beneficial effects of hESC-EPIs observed histologically also translated to an increase in contractility. EHT constructs were transferred to a myograph with a length controller and a force transducer (Supplementary Fig. 5a); constructs containing CMs and hESC-MSCs or primary MSCs or hESC-EPIs exhibited a Frank–Starling relationship, where twitch force increased linearly with increasing preload. In line with the histological finding that high-purity CMs alone do not result in efficient tissue remodeling, CM maturation or electrical connectivity, we did not observe coordinated contraction or measurable force production in 3D-EHTs containing CMs alone. Constructs containing hESC-EPIs produced the greatest total force amongst the four groups. Additionally, EHTs containing hESC-EPIs showed the greatest increase in active force production with increasing strain (that is, the greatest contractility) compared with primary MSCs and hESC-MSCs (Fig. 2a and Supplementary Fig. 5b). At the same time, 3D-EHTs containing hESC-EPIs produced the least passive force compared with primary MSCs or hESC-MSCs, which would correspond to a more compliant tissue with better relaxation potential during diastole (Fig. 2b).

When assessing the Ca^{2+} handling of the constructs, those containing hESC-EPIs and primary MSCs accounted for the most mature Ca^{2+} transients (Fig. 2c,d). Constructs containing EPDCs had more rapid Ca^{2+} release and Ca^{2+} decay compared with those with primary MSCs (Fig. 2e and Supplementary Fig. 5c, d). Constructs containing hESC-MSCs displayed irregular and broad Ca^{2+} transients, reflecting less coordinated beating. In those containing CM-only, no coordinated Ca^{2+} transients were detectable, but rather asynchronous contraction of single non-connected CMs was observed, which translated to noise in multicellular regions of interest.

Next, we tested whether the ability of epicardial cells to promote 3D-EHT function is independent of the parental hESC line. We generated EHTs where CMs and EPDCs were differentiated from the same H9 line, as well as with CMs from H9 cells and EPDCs from RUES2 hESCs. In both contexts, the EPDC-containing EHTs showed superior contractility and Ca^{2+} dynamics compared with EHTs made with hESC-MSCs or primary MSCs. These experiments demonstrated that enhancement of EHT function by EPDCs is a general attribute of epicardial cells and not a line-dependent artifact (Supplementary Figs. 6a,b and 7a–d).

Furthermore, in a separate experiment we determined the nature of the non-CM population obtained on differentiation of high-purity CMs by flow cytometry using markers previously described[32]. We found positivity for THY1 and PDGFR-β and to a minor degree for CD31 and NKX2.5 in this cTnT-negative cell population (Supplementary Fig. 8). Overall, this demonstrated a mesenchymal and fibroblast-like nature to these non-CMs and was comparable between RUES2- and H9-derived cells.

In conclusion, hESC-EPIs promote functional maturation of 3D-EHT. These findings encouraged us to explore their use in vivo as an adjunct to CM transplantation for cardiac repair.

Epicardial cells engraft and differentiate in the myocardial infarct. To assess the response of hESC-EPIs to engraftment in vivo we performed a series of pilot transplants into the infarct zone of athymic rats (Supplementary Fig. 9a). Because most non-myocytes that are transplanted into the heart rapidly die[33], we subjected the epicardial cells to heat shock and a prosurvival cocktail (PSC) of anti-apoptotic and anti-necrotic factors. At 7 d post-transplantation we found small grafts in 3 of 4 animals receiving 2×10^6 cells and larger grafts in all 4 animals receiving 4×10^6 cells (Supplementary Fig. 9b, c). To maximize survival at 28 d post-transplantation, we delivered 6×10^6 cells and found large grafts in 6 of 6 animals (Supplementary Fig. 9d), indicating that the grafts survive long term. We confirmed in a separate experiment that delivery with heat shock + PSC is required for engraftment of epicardial cells (Supplementary Fig. 10a–c). Conversely,

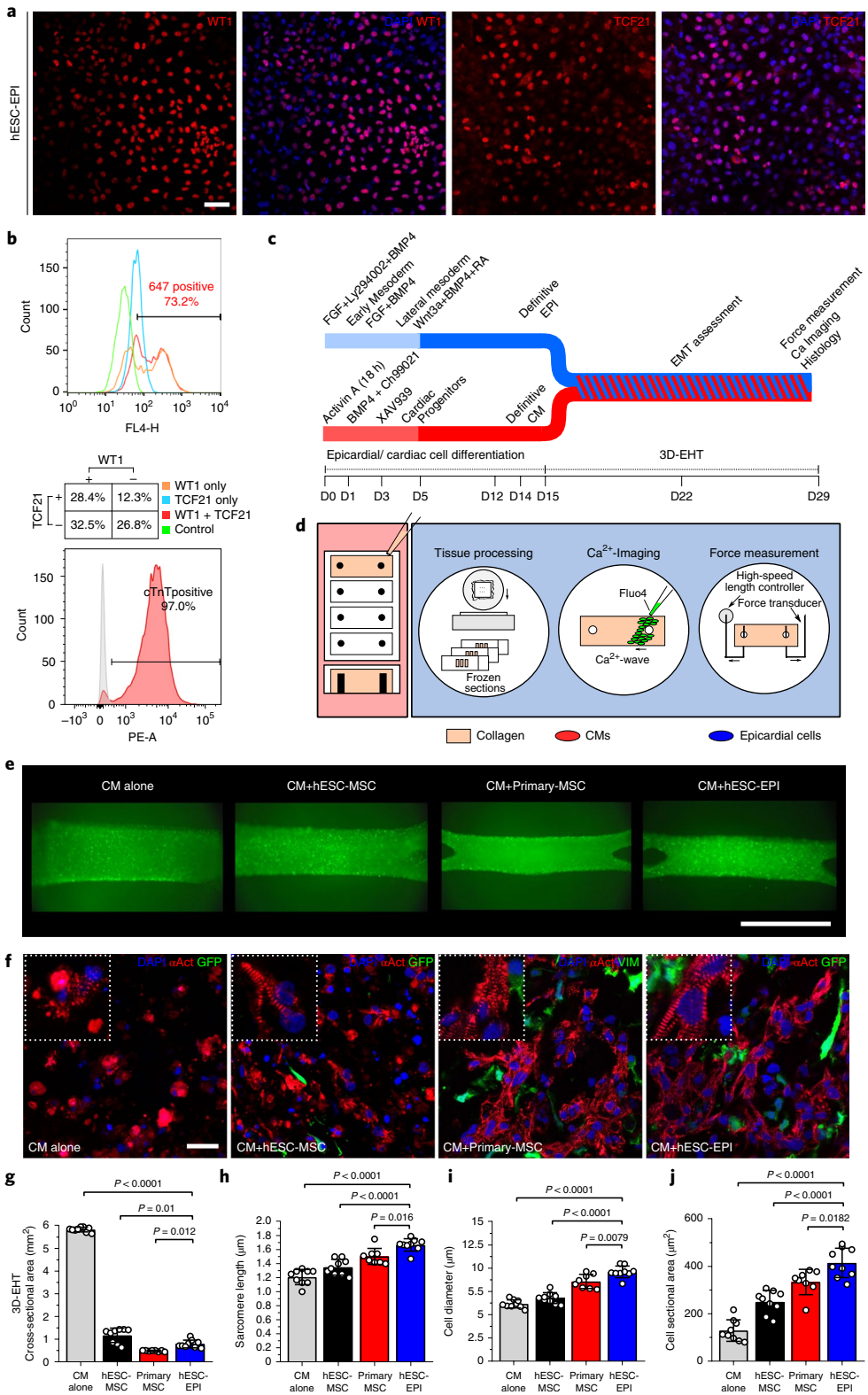

Fig. 1 | Generation and maturation of 3D-EHTs using hESC-EPIs and CMs. a, Epicardial cells derived from hESCs expressing the epicardial markers WT1 and TCF21. Scale bar, 50 μm. **b**, Purity of epicardial cells and CMs by flow cytometry. Control groups represent secondary and isotype antibodies for epicardial cells and CMs, respectively. Flow cytometric analysis was independently repeated three times with similar results. **c**, Schematic of experimental design. Epicardial cells and CMs were derived from hESCs and cocultured in 3D-EHT. **d**, Schematic of 3D-EHT using hESC-EPIs and CMs. **e**,**f**, Compaction (**e**) and ultrastructure (**f**) of 3D-EHT containing CMs alone, CM + hESC-MSC, CM + Primary MSC or CM + hESC-EPI. Scale bars, 2.5 mm and 25 μm. **a**,**e**,**f**, Experiments were independently repeated nine times with similar results. **g**–**j**, Quantification of tissue remodeling (**g**), sarcomeric length (**h**), cell diameter (**i**) and cell sectional area (**j**). Mean values; error bars represent s.d. Two-sided *P* values were calculated using a one-way ANOVA with post-hoc correction for multiple comparisons. CM alone, CM + hESC-MSC, CM + Primary MSC and CM + hESC-EPI, $n = 9, 9, 8, 9$ constructs, generated independently and measured on 3 different days. D, day; FL4-H and PE-A, fluorescence channels.

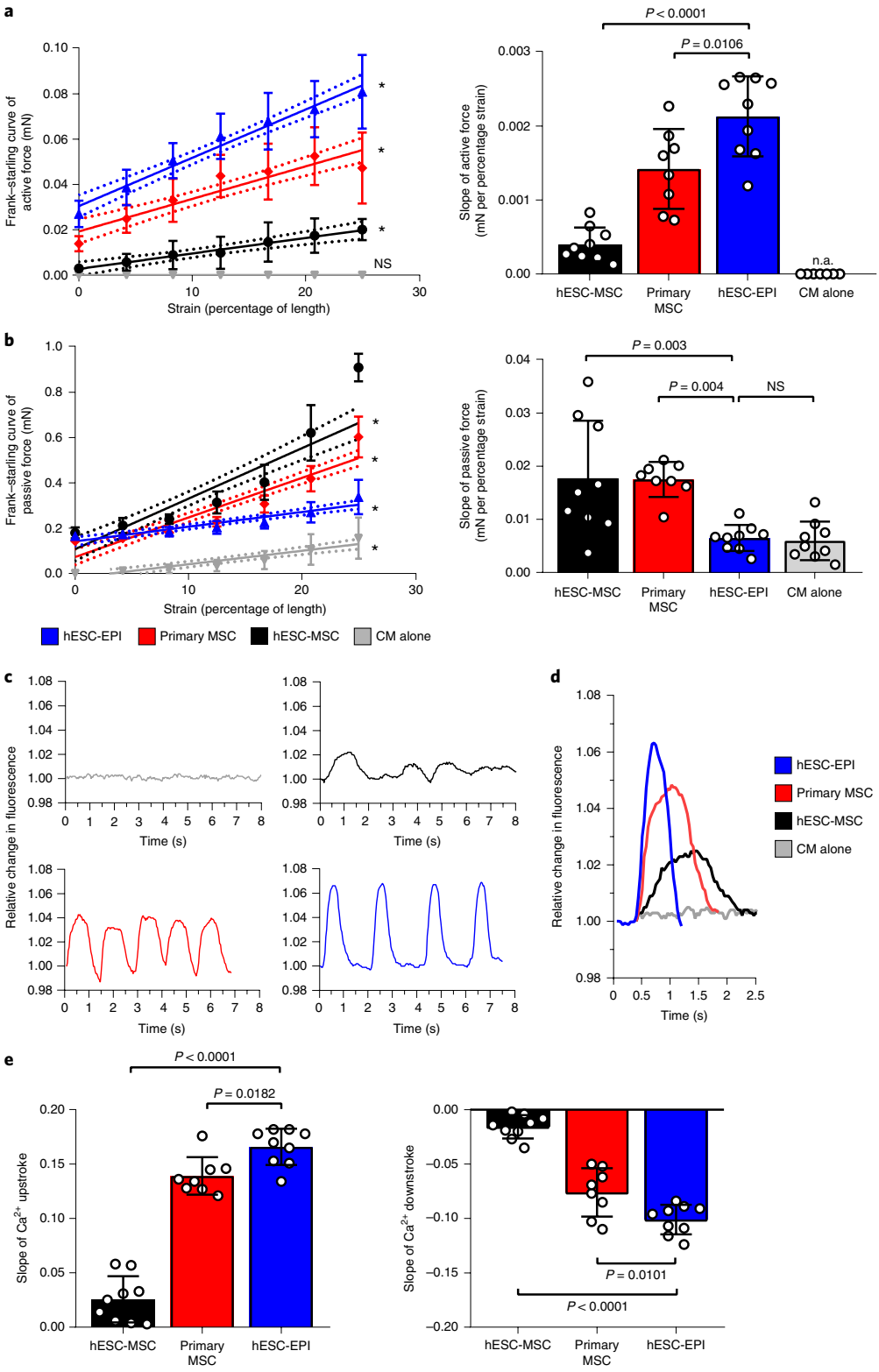

Fig. 2 | hESC-EPIs promote contractility and Ca^{2+} handling of 3D-EHTs. a, Active force generation of 3D-EHT containing CMs alone, CM + hESC-MSC, CM + Primary MSC or CM + hESC-EPI. Displayed are the Frank–Starling curve of active force production and the slope of the generated curve, respectively. **b**, Passive force of 3D-EHT containing CMs alone, CM + hESC-MSC, CM + Primary MSC or CM + hESC-EPI. Displayed are the curve of passive force production and the slope of the generated curve, respectively. **c**, Representative Ca^{2+} traces of 3D-EHT. **d**, Overlay of representative Ca^{2+} curves. **e**, Slope of Ca^{2+} upstroke and Ca^{2+} downstroke. Mean values; error bars represent s.d. Dotted lines represent 95% confidence intervals. Two-sided *P* values were calculated using a one-way ANOVA with post-hoc correction for multiple comparisons. CMs alone, CM + hESC-MSC, CM + Primary MSC and CM + hESC-EPI, $n = 9$, 9, 8 and 9 constructs, generated independently and measured on 3 different days. n.a., not applicable; NS, not significant.

epicardial cell transplantation in NOD scid gamma mice, without heat shock + PSC, demonstrated no detectable graft formation at 28 d (Supplementary Fig. 11a–c).

At 7 d post-transplantation the EPDCs coexpressed pan-cytokeratin and vimentin, indicating ongoing EMT. At 28 d post-transplantation EMT was essentially complete, with all grafted cells expressing vimentin and almost no detectable expression of pan-cytokeratin (Supplementary Fig. 9e,f). A small subpopulation of grafted vimentin-positive cells coexpressed WT1 on day 7 and day 28. This reflects the human fetal heart, where activated vimentin$^+$ epicardial cells invade the compact myocardium with a subpopulation retaining WT1 expression (Supplementary Fig. 9g,g'). At 28 d the grafted epicardial cells expressed S100A4, suggesting a fibroblast phenotype, whereas they neither expressed SM22α nor integrated into blood vessel walls, (Supplementary Fig. 12a,b). Grafted cells were negative for the cardiac marker α-actinin and the endothelial marker human lectin (Supplementary Fig. 12c–e). Taken together, these data indicate that EPDCs differentiate into cardiac fibroblast-like cells with no formation of CMs, endothelial cells or smooth muscle cells.

Because EPDCs readily form smooth muscle cells in vitro, we hypothesized that the infarct environment inhibited this differentiation pathway. To test this, we delivered hESC-EPIs in PSC onto the chorionic vasculature of chick embryos. After 5 d the human EPDCs had integrated into the walls of host vessels and expressed SM22α (Supplementary Fig. 13a–c). Thus, epicardial cells are multipotent and in an embryonic environment readily differentiate into vascular smooth muscle, whereas in the adult infarct they form fibroblast-like cells.

Cotransplantation of epicardial cells and CMs augments microvascular density. The long-term persistence of hESC-EPIs in infarcted hearts led us to hypothesize that these cells would exhibit a trophic effect on grafted hESC-CMs and the host myocardium. To test this, we performed a cotransplantation study where 4 groups of athymic rats received an injection of 5×10^6 hESC-EPIs, 10×10^6 hESC-derived CMs, the combination of both (EPI + CM: 5×10^6 hESC-EPIs plus 10×10^6 CMs) or vehicle control (PSC; Fig. 3a). At 4 weeks post-transplantation no difference in infarct size was found between the groups, ruling out effects on infarct scar healing (Fig. 3b,c).

To assess whether cell transplantation had an effect on host vessel recruitment, we quantified the microvascular density in the cardiac grafts, the infarct zone and the non-injured border zone (Fig. 3d). Microvascular density was significantly increased in cardiac grafts of animals that were cotransplanted with epicardial cells and CMs. Furthermore, erythrocytes were readily detectable in the lumens of the vessels, indicating perfusion via the coronary circulation (Fig. 3e and Supplementary Fig. 14a). We also observed an increase in microvascular recruitment in the infarct zone and in the non-injured border zone of the infarct, which was highest in EPI + CM, followed by CM, then EPI and finally vehicle control (Fig. 3f,g). To assess the timing of microvascular sprouting we made use of our pilot trial data set, and demonstrated that epicardial cells alone led to a significant increase in microvascular density in the infarct and border zones by day 28 but not by day 7 post-transplantation, indicating delayed angiogenic effects (Supplementary Fig. 14b–e).

To address the maturity of neo-vessels we also screened the three areas of interest for presence of smooth muscle cell-coated arteries. Vessels containing SM22α$^+$ mural cells were abundant in the infarct zone and the border zone of all groups. However, when assessing their presence within cardiac grafts we observed smooth muscle cell-coated vessels in the EPI + CM group but not in the CM-alone group, suggesting that epicardial cells promote smooth muscle encoatment and vascular maturation within the graft (Supplementary Fig. 14f–k). Absence of costaining for SM22α and human mitochondria further confirmed that the smooth muscle coats were rat-derived, and that epicardial cells were also not able to differentiate to smooth muscle cells in the infarct zone in the presence of CMs (Supplementary Fig. 14l). In summary, hESC-EPIs create a more highly vascularized cardiac graft, and microvascular density surrounding scar and border zones, which should promote a more favorable niche for hESC-CM engraftment and function.

Cotransplantation promotes cardiac graft size, proliferation and maturity. We next assessed the effects of epicardial cells on the cardiac grafts. Given the trophic effects of epicardial cells on CMs in vitro, we first investigated whether cotransplantation would affect cardiac graft size. Cardiac grafts were readily identified with antibodies directed against β-MHC (MYH7; whereas rat CMs predominantly express α-MHC/MHY6) and coexpressed α-actinin. Cardiac grafts were 2.6-fold larger when CMs were cotransplanted with epicardial cells, compared with CMs alone, averaging $3.9\pm1.6\%$ of the left ventricle versus $1.5\pm0.9\%$ of the left ventricle, respectively (Fig. 4a,b and Supplementary Fig. 14m).

Because epicardial cells secrete growth factors for CMs during development, we hypothesized that epicardial cells augmented graft size via increased CM proliferation. All rats in this phase of the study were pulsed with the thymidine analog, BrdU, on 1, 3, 7 and 14 d post-cell delivery. To determine cumulative proliferation rates in the grafts we stained with antibodies directed against BrdU and the human-specific cardiac marker β-MHC. The proliferative index of β-MHC-positive cells was twofold higher in animals that received the combination of hESC-EPIs and CMs ($8\%\pm1.4\%$) compared with CMs alone ($4\pm0.9\%$, $P<0.0001$; Fig. 4c,d). Conversely, there was no difference in the proliferative index of vimentin-positive EPDCs in animals receiving epicardial cells alone or epicardial cells with CMs (Supplementary Fig. 15a,b). Taking the graft CM BrdU rates as daily averages of DNA synthesis, and assuming that the cell cycle lasts 24 h, hESC-CM graft expansion can be calculated for each group. For 28-day grafts, control expansion would be 1.04×10^{28}, or 3.0-fold expansion, while in cotransplantation studies it would be 1.08×10^{28}, or 8.6-fold expansion. This predicts a 2.9-fold difference in graft size, which is quite close to our observed 2.6-fold difference. Thus, although we cannot rule out a role for increased graft survival, these data indicate that enhanced CM proliferation is a major driver for the increased CM graft size observed with hESC-EPI cotransplantation.

Given the epicardial effects on CM maturation in vitro, we assessed the sarcomere length of the cardiac grafts. In line with our findings in vitro, CMs that were cotransplanted with epicardial cells exhibited a greater sarcomeric length and cell diameter as well as a 77% larger cell sectional area (Fig. 4f–h) than those that were transplanted alone, indicative of a more mature phenotype. Additionally, we demonstrated that cotransplantation of CMs with epicardial cells leads to an isoform switch from ssTnI to cTnI in cardiac grafts (Fig. 4e).

As cardiac fibrosis impedes structural integration of grafts and host[34], we were concerned that epicardial cell-derived fibroblasts might interfere with gap junctions between graft and host CMs. To investigate this, we performed combined immunostaining for β-MHC, cTnT and the gap junction protein connexin 43. Gap junctions between graft and host were seen in multiple areas across all animals, demonstrated by connexin 43 expression between neighboring human and rat CMs (Fig. 4i). While epicardial cells themselves can express connexin 43 (refs. [35,36]), the gap junctions identified in our study were predominantly between CMs. In conclusion, hESC-EPIs promote cardiac graft size, in part through proliferation, and enhance maturation/myofibril development while still permitting structural integration of grafted CMs with the recipient myocardium.

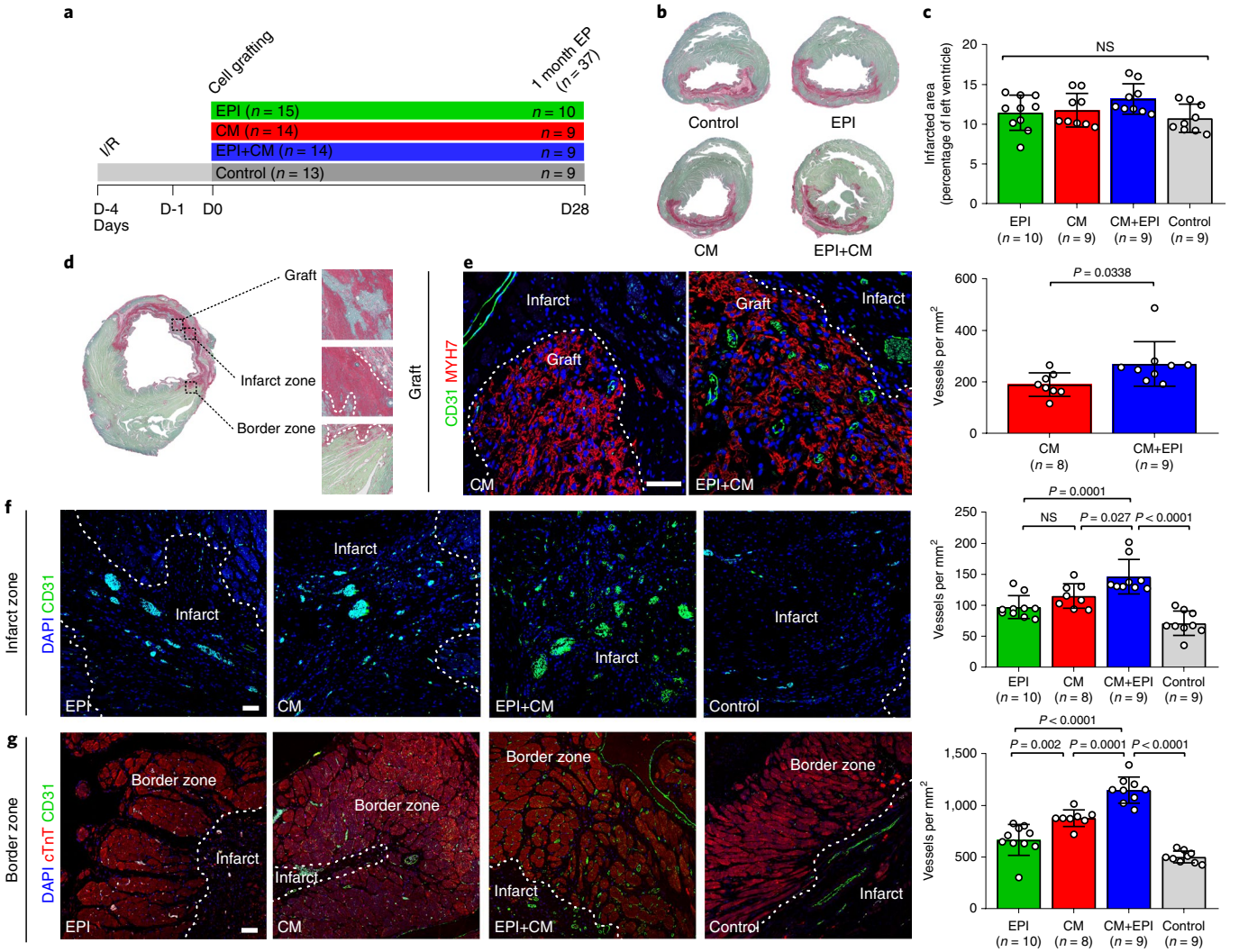

Fig. 3 | Cotransplantation of hESC-EPIs with CMs promotes microvascular density. a, Schematic of study design. **b**, Representative picrosirius red/fast-green counterstained infarcted rat heart sections. **c**, Quantification of myocardial infarct size. $N=37$ in total for histologic analysis of infarct size at the 1-month time point. *n* represents the number of animals. **d**, Schematic of areas assessed for vascularization. **e**, Microvascular density in cardiac grafts. **f**, Microvascular density in the infarct zone. **g**, Microvascular density in the non-injured border zone of the infarct. Due to the presence of erythrocyte autofluorescence all quantification was performed manually to avoid erroneous detection with automated software. Mean values; error bars represent s.d. Two-sided *P* values were calculated using a one-way ANOVA with post-hoc correction for multiple comparisons unless otherwise stated. $N=36$ in total for histologic analysis at the 1-month time point since 1 animal in the CM group did not exhibit a cardiac graft. Control, EPI, CM and CM + EPI, $n=9$, 10, 8 and 9 animals. Scale bars, 50 µm. I/R, ischemia/reperfusion.

Cotransplantation promotes cardiac function. To assess the functional effects of cardiac grafts on global host heart function, we performed cardiac ultrasound on all animals before infarction, immediately before cell injection and after 28 d follow-up. The ultrasound scans (A.M.) and their interpretations (J.B. and F.W.) were performed by investigators who were blinded to the treatment to prevent bias. All groups exhibited comparable left ventricular dilation and decline in left ventricular function after infarction, consistent with the histological finding of comparable infarct sizes (Fig. 5a–c and Supplementary Table 1). Compared with their pre-injection (postinfarction) baseline values, the vehicle control group displayed a $9\pm5.4\%$ decline in fractional shortening by 4 weeks after injection, indicating a progression toward heart failure ($P<0.0001$ versus baseline). The EPI group showed a $5.3\pm6.5\%$ decline in fractional shortening. Similar to previous reports from our group[8], transplantation of only CMs preserved cardiac function over the 4-week period, indicating that CM transplantation prevented the progression to heart failure. Notably, animals receiving combined CM + EPI grafts showed a $4.5\pm3.6\%$ improvement in fractional shortening, indicating that cotransplantation significantly improved left ventricular function ($P=0.0175$ versus CMs only). Furthermore, we demonstrated that in the CM and CM + EPI groups improvements in left ventricular function correlate linearly with graft size (Supplementary Fig. 15c).

Comparing pre- and postinjection values, left ventricular end systolic dimension (LVESD) remained stable in the CM + EPI group and increased in the CM only group, followed by greater increases in the EPI and the vehicle control group. The change in LVESD in the CM + EPI group was significantly smaller than in the vehicle control group but the difference to the CM only group or the EPI group did not reach statistical significance (Fig. 5d,e). For left ventricular end diastolic dimension (LVEDD), analysis of variance (ANOVA) did not yield a significant difference (Fig. 5f,g). Taken together, these studies show that cotransplantation of hESC-EPIs

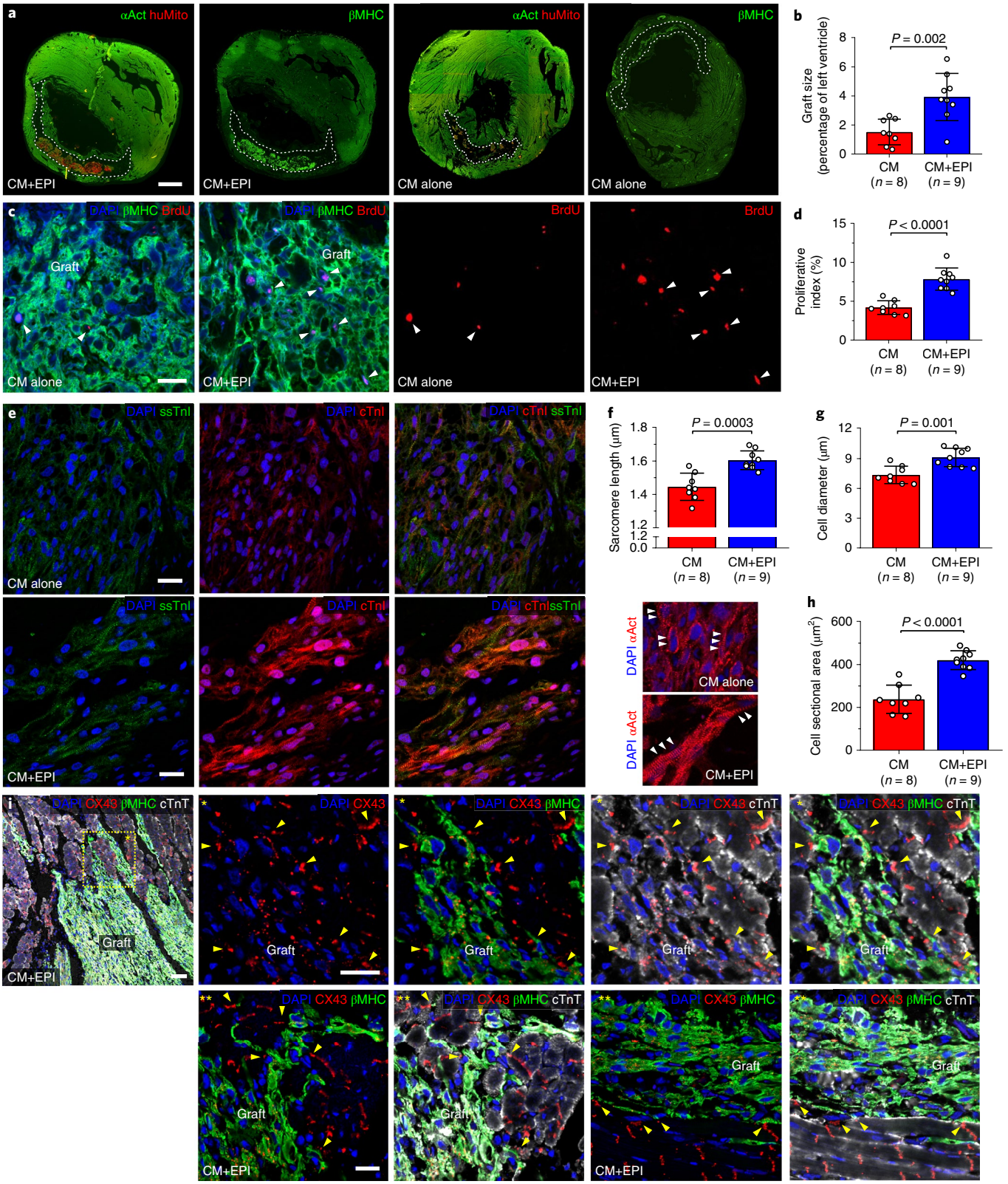

Fig. 4 | hESC-EPIs potentiate cardiac regeneration. a, Representative sections of infarcted hearts demonstrating the cardiac grafts in animals that received either hESC-EPIs and CMs or CMs alone. βMHC is specific for grafted human CMs while αAct antibody stains both rat and human CMs. Scale bar, 2.5 mm. **b**, Quantification of cardiac graft size. **c**, Proliferative index of human CMs in cardiac grafts. Scale bar, 20 μm. **d**, Quantification of proliferative index. **e**, Isoform switch of ssTnI to cTnI in CMs in vivo in animals receiving EPI + CM and CM alone. Staining performed in five animals per group. Scale bars, 20 μm. **f**, Quantification of sarcomeric length. **g**, Quantification of cell diameter in CMs in vivo. **h**, Quantification of cell sectional area in CMs in vivo. **i**, Cardiac grafts and Cx43$^+$ gap junctions with host tissue. Scale bars, 50 μm for **i** and 20 μm for * and **. **i**, CX43 staining was performed on all animals. Mean values; error bars represent s.d. Two-sided *P* values were calculated using an unpaired *t*-test unless otherwise stated. $N = 17$ in total for histologic analysis of cardiac grafts after 1 month; CM and CM + EPI, $n = 8$ and 9 animals.

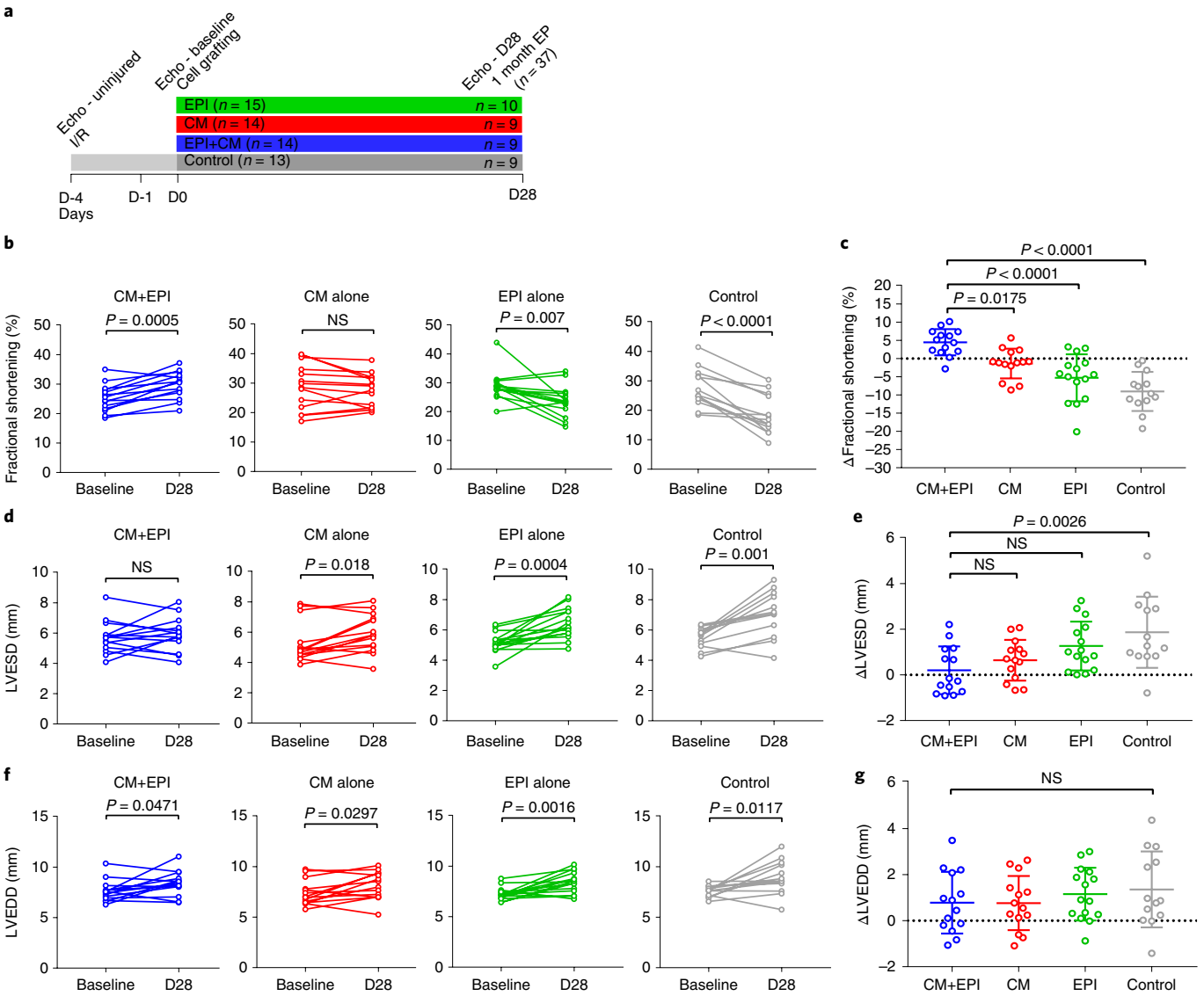

Fig. 5 | Cotransplantation of epicardial cells and CMs promotes functional recovery. a, Schematic of study design and timing of echocardiographic data collection. **b**, Echocardiographic effects of hESC-EPI augmented cardiac grafts on postinfarct ventricular function. Fractional shortening values are given for the 96 h pretreatment baseline and 1-month follow-up. **c**, Difference in fractional shortening. **d**, LVESDs are given for the 96 h pretreatment baseline and 1-month follow-up. **e**, Difference in LVESD. **f**, LVEDDs are given for the 96 h pretreatment baseline and 1-month follow-up. **g**, Difference in LVEDD. Mean values; error bars represent s.d. Two-sided *P* values were calculated using a paired *t*-test for comparison of cardiac function within groups between baseline and 1-month follow-up. If more than two groups were compared, a one-way ANOVA with post-hoc correction for multiple comparisons was used. $N = 56$ in total for functional analysis after 1 month; control, EPI, CM and CM + EPI, $n = 13$, 15, 14 and 14 animals. EP, endpoint.

with CMs leads to a greater increase in cardiac function compared with transplantation of CMs alone. Furthermore, this benefit manifests principally as enhanced systolic function rather than impacting left ventricular remodeling.

To investigate whether these effects would be present in the long term, we followed a subset of 4–5 animals per group for up for 3 months. Three months after cell grafting, hESC-EPIs as well as hESC-derived CMs were still present in the infarct zone as confirmed by anti-human mitochondrial staining (Supplementary Fig. 16a–c). In line with the 28-d follow-up, at 84 d post-transplantation no differences were found in infarct size between the 4 study groups (Supplementary Fig. 16d). Functional analysis demonstrated long-term perpetuation of benefits perceived at 1 month due to persistent systolic improvement. Fractional shortening showed no decline in animals receiving CM + EPI or CM only but a significant decline in animals receiving either EPI or vehicle control. While there was no difference in the change of fractional shortening between day 28 and day 84 among the groups, the change occurring between day 4 and day 84 was significantly greater in the CM + EPI group compared with CMs only, EPIs only or vehicle control (Supplementary Fig. 16e,f). Indeed the 4.5% improvement in fractional shortening at 4 weeks for epicardial cell cotherapy over CMs alone increased further to 9.6% by 12 weeks (Supplementary Fig. 16f). To summarize, hESC-derived cellular grafts and related functional improvement in cardiac function persist in the long term.

RNA sequencing reveals the epicardial secretome. Finally, to address the question of putative mediators of epicardial cell-driven cardiac repair we performed RNA sequencing of hESC-derived epicardium as used for all in vitro and in vivo experiments. In embryonic heart development, the neural crest is essential for pharyngeal arch organization and outflow tract septation, but

lineage-tracing studies have to date not suggested a role in cardiac maturation[37–39]. We first used hESC-derived neural crest cells in 3D-EHTs, demonstrating the inability of this cell population to result in structural and functional heart maturation, in contrast to epicardial cells (Supplementary Fig. 17a,b). We therefore used neural crest cells as a negative control for RNA sequencing (Fig. 6a and Supplementary Table 2).

As epicardial cells resulted in stark effects on tissue remodeling of 3D-EHTs and because it has been demonstrated that the extracellular matrix (ECM) plays a key role in epicardial-driven heart repair, we focused on ECM molecules secreted by epicardial cells and differentially expressed in the hESC-derived neural crest cells (Supplementary Table 2). The heatmap shown in Fig. 6a displays differentially expressed genes with an adjusted $P < 1 \times 10^{-7}$ (a complete list of the genes and their expression is shown in Supplementary Table 2). Amongst them, fibronectin is one of the most differentially expressed candidates. We then performed a gene ontology enrichment analysis, which further highlights a potential role for ECM expressed by hESC-EPIs in myocardial development and maturation (Fig. 6b,c and Supplementary Fig. 18).

We first demonstrated that fibronectin was also abundantly expressed at the protein level in 3D-EHTs containing epicardial cells but to a lesser degree in constructs containing hESC-MSCs, primary MSCs or CMs alone (Fig. 6d). Furthermore, fibronectin was highly expressed in cardiac grafts in vivo in animals receiving epicardial cells and CMs or epicardial cells alone, but only at a rudimentary level in those receiving CMs alone or vehicle control (Fig. 6e). In summary, RNA sequencing has provided the secretome of hESC-derived epicardium and identified a potential involvement of ECM remodeling in the process of cardiac maturation in vitro and in vivo. These data provide a valuable target library for future cardiac repair strategies.

Discussion

This study was designed to address two gaps in knowledge: the immaturity of hPSC-derived CMs, and the inefficient remuscularization of infarcts following hPSC-CM transplantation. Because of the key trophic role played by the epicardium during development, we hypothesized that hPSC-epicardial cells would promote CM proliferation and maturation, resulting in better EHT formation in vitro and better infarct remuscularization in vivo. We found that hESC-EPIs undergo EMT to fibroblast-like cells both in vitro and in vivo. In EHTs EPDCs augment tissue structure and function, resulting in increased CM size, sarcomere length and force production, and augmented Ca^{2+} handling. When codelivered with hESC-CMs into myocardial infarcts, EPDCs stimulate hESC-CM proliferation, increasing remuscularization by 2.6-fold. Additionally, EPDCs stimulate vascularization within the graft and infarct scar and in the border zone host myocardium. These changes are accompanied by remodeling of the ECM, including high levels of fibronectin deposition. Finally, codelivery of hESC-derived epicardium with hESC-CMs results in significantly improved ventricular function postinfarction.

The pivotal role of the epicardium in heart development is well recognized. During early embryonic heart formation the epicardial tissue gives rise to coronary smooth muscle cells[22,23] and myocardial fibroblasts[24,25,40]. While smooth muscle cells are critical for formation of the coronary vasculature, cardiac fibroblasts are essential for myocardial proliferation and compaction[26]. Conversely, inhibiting proepicardial outgrowth results in pathologic formation of the coronary vessels and non-compaction cardiomyopathy[41]. The trophic effect of quail and rat EPDCs has been demonstrated in coculture experiments resulting in structural and functional maturation of CMs[27,29]. Our data show that coculture of hESC-EPIs and CMs results in compaction and structural as well as functional maturation of 3D-EHT. More specifically, we demonstrate that hESC-derived epicardium outcompetes both hESC-derived MSCs as well as primary MSCs in terms of force generation and Ca^{2+} handling, corroborating the functional role of its embryonic identity. The functional potency of epicardial cells might prove broadly applicable to current tissue engineering strategies, which would benefit from enhanced structural integrity and function of CMs[42].

In neonatal mice and in zebrafish, the epicardium is thought to have a key role in facilitating myocardial regeneration following injury[43,44]; in contrast, the adult mammalian heart displays inadequate epicardial activation and fails to regenerate myocardium postinjury. In this context it has been demonstrated that embryonic cardiac fibroblasts induce greater cardiac proliferation than their adult counterparts[26]. Consequently, we propose that the fetal-stage epicardium generated by hESCs may preferentially promote regeneration.

It is important to consider the mechanism of action through which the epicardial cells improve the impact of CM transplantation. Since CMs are already effective by themselves, the 2.6-fold enhancement of CM engraftment induced by epicardial cell codelivery may underlie much of the benefit on cardiac function. The positive correlation of cardiac graft size and percentage change in fractional shortening corroborates this interpretation (Supplementary Fig. 15c). Most of this increase in engraftment can be accounted for by the twofold increase in CM DNA synthesis rates induced by epicardial cell codelivery, although beneficial effects on CM survival cannot be ruled out. Another important factor, however, is that the EPDCs induced a substantial amount of angiogenesis in the graft, infarct scar and border zone host myocardium. Increased vascularization should improve the function of both graft and host tissues and could contribute to the beneficial effect.

A third potential mechanism was raised by our RNA-sequencing studies, which demonstrated that hESC-EPIs synthesize an embryonic ECM that is particularly rich in fibronectin. It has been demonstrated that the secretion of fibronectin by epicardial cells is required for heart regeneration in zebrafish[45]. In line with these findings it was demonstrated that the orchestrated secretion of fibronectin, collagen and heparin-binding EGF-like growth factor by embryonic but not adult fibroblasts resulted in CM proliferation[26]. We therefore propose that the matrix laid down by hESC-EPIs is likely to exhibit developmental cues that are absent in mature postinfarct myocardium, providing an advantageous niche in a hostile environment; the gene ontology analyses of RNA-sequencing data are in support of this. Further elucidation of the observed cross-talk between epicardium and CMs might aid ongoing tissue engineering and cell therapy endeavors, and the extensive data on epicardially expressed genes made available here provide a rich resource for further study. These mechanisms are not mutually exclusive and could coexist.

Finally, although we favor the notion that the salutary effects of codelivering CMs plus epicardial cells result from the impact on CM graft size, vascularization and ECM, we cannot rule out a paracrine effect from simply increasing the number of delivered cells in the combined cell group. Indeed, our data do not permit distinguishing the direct mechanical effects of the CM grafts from the paracrine factors they secrete; presumably, both mechanisms may coexist and be augmented by larger CM grafts. However, this does not detract from our primary conclusion that hESC-EPIs recapitulate their embryonic role in the post-myocardial infarction setting by promoting hESC-derived CM proliferation and maturity and at the same time favorably influencing host tissue regeneration.

Two other studies have demonstrated that human primary epicardial cells improve function of the infarcted heart and that cotransplantation of adult cardiovascular progenitors with epicardial cells exerts a synergistic effect that exceeds that of monotherapy[33,46]. There were several important differences with our study, including their use of epicardial cells and cardiac progenitor cells derived from the adult human heart (versus our use of hESC derivatives)

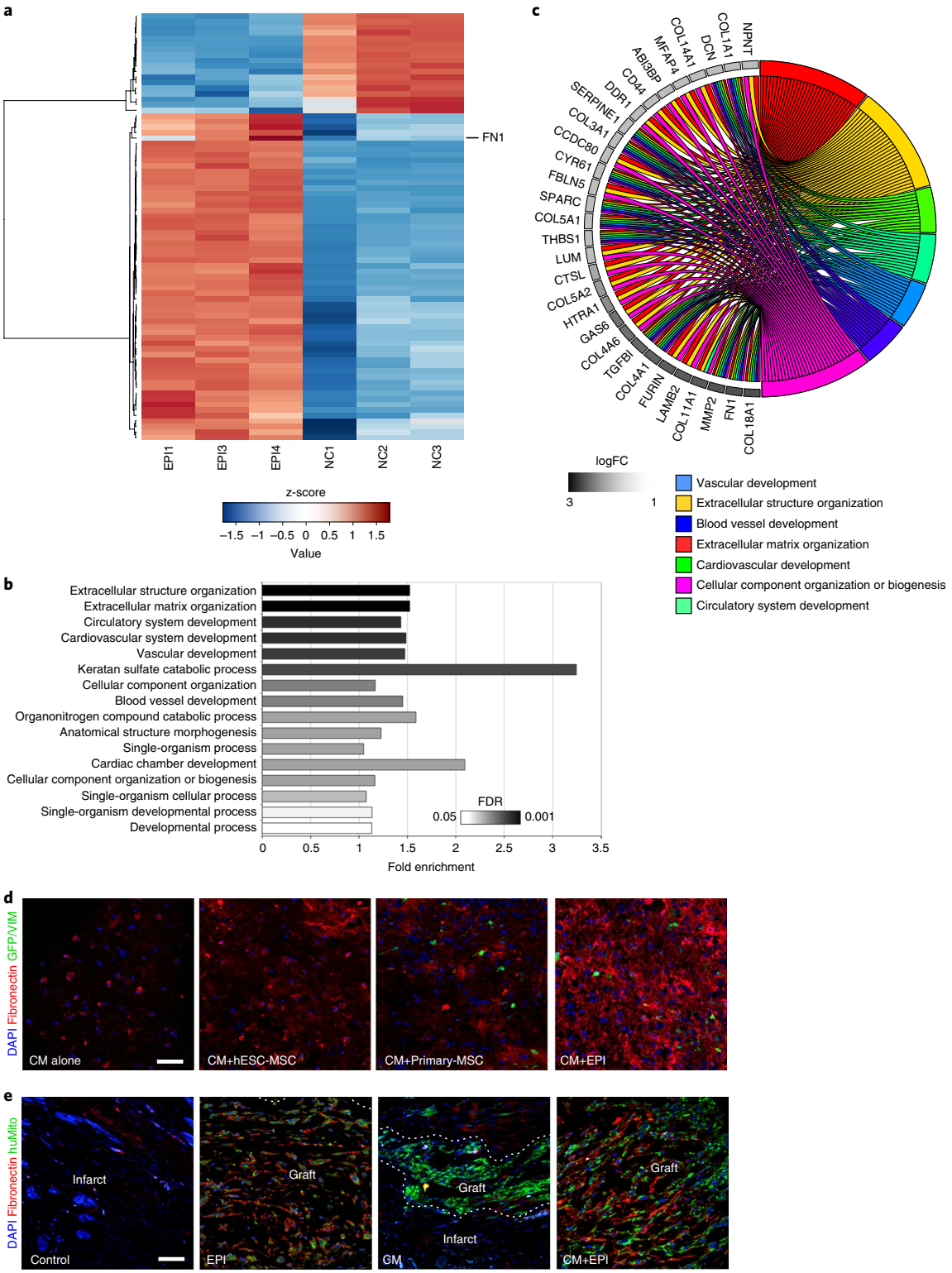

Fig. 6 | Epicardial secretome. a, Heatmap depicting differentially expressed secreted factors in epicardial cells compared with neural crest. **b**, Gene enrichment analysis showing the top enriched gene ontology biological processes. The 705 genes specifically enriched in the EPI secretome were subjected to a hypergeometric test against a background of the 2,413 secretome genes expressed in NC or EPI. Gene ontology terms are shaded between black and white based on their false discovery rate after Benjamini–Hochberg correction. **c**, Circular gene ontology plot depicting the top gene ontology terms enriched in EPI versus NC associated with at least ten genes on the right and the associated genes on the left. Genes are shaded between black and white based on their fold enrichment in EPI compared with NC. **a**–**c**, EPI and NC, $n = 3$ and 3. **d**, Fibronectin expression in 3D-EHT in vitro. CM alone, CM + hESC-MSC, CM + Primary MSC and CM + hESC-EPI, $n = 9$, 9, 8 and 9 constructs, generated independently. Scale bars, 50 µm. **e**, Fibronectin expression in epicardial and cardiac grafts in animals in vivo. Scale bars, 50 µm. This staining was performed on all animals at the 1-month time point ($n = 37$). NC, neural crest. FC, fold change; FDR, false discovery rate.

and their use of NOD-SCID mice with permanent coronary ligations (versus our use of athymic rats with ischemia-reperfusion injury). While these results demonstrated a beneficial effect of polycell therapy, the authors did not detect stable grafts in any of the groups, indicating that the effects seen were paracrine in nature. Indeed, we are not aware of any studies in the literature that have demonstrated robust CM and supportive cell-type engraftment in the long term following myocardial infarction. In contrast, our grafts, both cardiac as well as epicardial, and related functional benefits were detectable up to 3 months post-transplantation, providing evidence for longevity and potential perpetuation of benefits in the long term.

In conclusion, hESC-EPIs are a promising tool to advance regenerative cardiovascular medicine, including cell transplantation as well as tissue-engineering strategies. Future studies are warranted to better understand the mechanisms through which epicardial cells propagate the observed benefits and to investigate their function in models that more closely match clinical application.

Online content

Any methods, additional references, Nature Research reporting summaries, source data, statements of code and data availability and associated accession codes are available at https://doi.org/10.1038/s41587-019-0197-9.

Received: 12 April 2017; Accepted: 24 June 2019;
Published online: 2 August 2019

References

1. Braunwald, E. Shattuck lecture—cardiovascular medicine at the turn of the millennium: triumphs, concerns, and opportunities. *N. Engl. J. Med.* **337**, 1360–1369 (1997).
2. Mozaffarian, D. et al. Heart disease and stroke statistics-2016 update: a report from the American Heart Association. *Circulation* **133**, e38–e360 (2016).
3. McMurray, J. J., Petrie, M. C., Murdoch, D. R. & Davie, A. P. Clinical epidemiology of heart failure: public and private health burden. *Eur. Heart J.* **19**, P9–P16 (1998).
4. Bertero, A. & Murry, C. E. Hallmarks of cardiac regeneration. *Nat. Rev. Cardiol.* **15**, 579–580 (2018).
5. Weinberger, F., Mannhardt, I. & Eschenhagen, T. Engineering cardiac muscle tissue: a maturating field of research. *Circ. Res.* **120**, 1487–1500 (2017).
6. Burridge, P. W. et al. Chemically defined generation of human cardiomyocytes. *Nat. Meth.* **11**, 855–860 (2014).
7. Lian, X. et al. Robust cardiomyocyte differentiation from human pluripotent stem cells via temporal modulation of canonical Wnt signaling. *Proc. Natl Acad. Sci. USA* **109**, E1848–E1857 (2012).
8. Laflamme, M. A. et al. Cardiomyocytes derived from human embryonic stem cells in pro-survival factors enhance function of infarcted rat hearts. *Nat. Biotechnol.* **25**, 1015–1024 (2007).
9. Patsch, C. et al. Generation of vascular endothelial and smooth muscle cells from human pluripotent stem cells. *Nat. Cell Biol.* **17**, 994–1003 (2015).
10. Orlova, V. V. et al. Generation, expansion and functional analysis of endothelial cells and pericytes derived from human pluripotent stem cells. *Nat. Protoc.* **9**, 1514–1531 (2014).
11. Cheung, C., Bernardo, A. S., Trotter, M. W., Pedersen, R. A. & Sinha, S. Generation of human vascular smooth muscle subtypes provides insight into embryological origin-dependent disease susceptibility. *Nat. Biotechnol.* **30**, 165–173 (2012).
12. Iyer, D. et al. Robust derivation of epicardium and its differentiated smooth muscle cell progeny from human pluripotent stem cells. *Development* **142**, 1528–1541 (2015).
13. Witty, A. D. et al. Generation of the epicardial lineage from human pluripotent stem cells. *Nat. Biotechnol.* **32**, 1026–1035 (2014).
14. Palpant, N. J. et al. Inhibition of beta-catenin signaling respecifies anterior-like endothelium into beating human cardiomyocytes. *Development* **142**, 3198–3209 (2015).
15. Palpant, N. J. et al. Generating high-purity cardiac and endothelial derivatives from patterned mesoderm using human pluripotent stem cells. *Nat. Protoc.* **12**, 15–31 (2017).
16. Shiba, Y. et al. Human ES-cell-derived cardiomyocytes electrically couple and suppress arrhythmias in injured hearts. *Nature* **489**, 322–325 (2012).
17. Weinberger, F. et al. Cardiac repair in guinea pigs with human engineered heart tissue from induced pluripotent stem cells. *Sci. Transl. Med.* **8**, 363ra148 (2016).
18. Chong, J. J. et al. Human embryonic-stem-cell-derived cardiomyocytes regenerate non-human primate hearts. *Nature* **510**, 273–277 (2014).
19. Shiba, Y. et al. Allogeneic transplantation of iPS cell-derived cardiomyocytes regenerates primate hearts. *Nature* **538**, 388–391 (2016).
20. Liu, Y. W. et al. Human embryonic stem cell-derived cardiomyocytes restore function in infarcted hearts of non-human primates. *Nat. Biotechnol.* **36**, 597–605 (2018).
21. van den Berg, C. W. et al. Transcriptome of human foetal heart compared with cardiomyocytes from pluripotent stem cells. *Development* **142**, 3231–3238 (2015).
22. Guadix, J. A., Carmona, R., Munoz-Chapuli, R. & Perez-Pomares, J. M. In vivo and in vitro analysis of the vasculogenic potential of avian proepicardial and epicardial cells. *Dev. Dyn.* **235**, 1014–1026 (2006).
23. Gittenberger-de Groot, A. C., Vrancken Peeters, M. P., Mentink, M. M., Gourdie, R. G. & Poelmann, R. E. Epicardium-derived cells contribute a novel population to the myocardial wall and the atrioventricular cushions. *Circ. Res.* **82**, 1043–1052 (1998).
24. Dettman, R. W., Denetclaw, W. Jr., Ordahl, C. P. & Bristow, J. Common epicardial origin of coronary vascular smooth muscle, perivascular fibroblasts, and intermyocardial fibroblasts in the avian heart. *Dev. Biol.* **193**, 169–181 (1998).
25. Manner, J. Does the subepicardial mesenchyme contribute myocardioblasts to the myocardium of the chick embryo heart? A quail-chick chimera study tracing the fate of the epicardial primordium. *Anat. Rec.* **255**, 212–226 (1999).
26. Ieda, M. et al. Cardiac fibroblasts regulate myocardial proliferation through beta1 integrin signaling. *Dev. Cell* **16**, 233–244 (2009).
27. Eid, H. et al. Role of epicardial mesothelial cells in the modification of phenotype and function of adult rat ventricular myocytes in primary coculture. *Circ. Res.* **71**, 40–50 (1992).
28. Stuckmann, I., Evans, S. & Lassar, A. B. Erythropoietin and retinoic acid, secreted from the epicardium, are required for cardiac myocyte proliferation. *Dev. Biol.* **255**, 334–349 (2003).
29. Weeke-Klimp, A. et al. Epicardium-derived cells enhance proliferation, cellular maturation and alignment of cardiomyocytes. *J. Mol. Cell. Cardiol.* **49**, 606–616 (2010).
30. Braitsch, C. M., Kanisicak, O., van Berlo, J. H., Molkentin, J. D. & Yutzey, K. E. Differential expression of embryonic epicardial progenitor markers and localization of cardiac fibrosis in adult ischemic injury and hypertensive heart disease. *J. Mol. Cell. Cardiol.* **65**, 108–19 (2013).
31. Ruan, J. L. et al. Mechanical stress conditioning and electrical stimulation promote contractility and force maturation of induced pluripotent stem cell-derived human cardiac tissue. *Circulation* **134**, 1557–1567 (2016).
32. Dubois, N. C. et al. SIRPA is a specific cell-surface marker for isolating cardiomyocytes derived from human pluripotent stem cells. *Nat. Biotechnol.* **29**, 1011–1018 (2011).
33. Winter, E. M. et al. A new direction for cardiac regeneration therapy: application of synergistically acting epicardium-derived cells and cardiomyocyte progenitor cells. *Circ. Heart Fail.* **2**, 643–653 (2009).
34. Gerbin, K. A., Yang, X., Murry, C. E. & Coulombe, K. L. Enhanced electrical integration of engineered human myocardium via intramyocardial versus epicardial delivery in infarcted rat hearts. *PloS ONE* **10**, e0131446 (2015).
35. van Tuyn, J. et al. Epicardial cells of human adults can undergo an epithelial-to-mesenchymal transition and obtain characteristics of smooth muscle cells in vitro. *Stem Cells* **25**, 271–278 (2007).
36. Bax, N. A. et al. Epithelial-to-mesenchymal transformation alters electrical conductivity of human epicardial cells. *J. Cell. Mol. Med.* **15**, 2675–2683 (2011).
37. Kirby, M. L., Gale, T. F. & Stewart, D. E. Neural crest cells contribute to normal aorticopulmonary septation. *Science* **220**, 1059–1061 (1983).
38. Porras, D. & Brown, C. B. Temporal-spatial ablation of neural crest in the mouse results in cardiovascular defects. *Dev. Dyn.* **237**, 153–162 (2008).
39. Jiang, X., Rowitch, D. H., Soriano, P., McMahon, A. P. & Sucov, H. M. Fate of the mammalian cardiac neural crest. *Development* **127**, 1607–1616 (2000).
40. Cai, C. L. et al. A myocardial lineage derives from Tbx18 epicardial cells. *Nature* **454**, 104–108 (2008).
41. Gittenberger-de Groot, A. C., Vrancken Peeters, M. P., Bergwerff, M., Mentink, M. M. & Poelmann, R. E. Epicardial outgrowth inhibition leads to compensatory mesothelial outflow tract collar and abnormal cardiac septation and coronary formation. *Circ. Res.* **87**, 969–971 (2000).
42. Ogle, B. M. et al. Distilling complexity to advance cardiac tissue engineering. *Sci. Transl. Med.* **8**, 342ps13 (2016).
43. Lepilina, A. et al. A dynamic epicardial injury response supports progenitor cell activity during zebrafish heart regeneration. *Cell* **127**, 607–619 (2006).
44. Porrello, E. R. et al. Transient regenerative potential of the neonatal mouse heart. *Science* **331**, 1078–1080 (2011).

45. Wang, J., Karra, R., Dickson, A. L. & Poss, K. D. Fibronectin is deposited by injury-activated epicardial cells and is necessary for zebrafish heart regeneration. *Dev. Biol.* **382**, 427–435 (2013).
46. Winter, E. M. et al. Preservation of left ventricular function and attenuation of remodeling after transplantation of human epicardium-derived cells into the infarcted mouse heart. *Circulation* **116**, 917–927 (2007).
47. Pittenger, M. F. et al. Multilineage potential of adult human mesenchymal stem cells. *Science* **284**, 143–147 (1999).

Acknowledgements

This work was supported by the British Heart Foundation (BHF; grants nos. NH/11/1/28922, G1000847, FS/13/29/30024 and FS/18/46/33663), Oxford-Cambridge Centre for Regenerative Medicine (grant no. RM/13/3/30159), the UK Medical Research Council (MRC) and the Cambridge Hospitals National Institute for Health Research Biomedical Research Centre funding (S.S.), as well as National Institutes of Health grant nos. P01HL094374, P01GM081619 and R01HL128362 and a grant from the Fondation Leducq Transatlantic Network of Excellence (C.E.M.). J.B. was supported by a Cambridge National Institute for Health Research Biomedical Research Centre Cardiovascular Clinical Research Fellowship and, subsequently, by a BHF Studentship (grant no. FS/13/65/30441). D.I. received a University of Cambridge Commonwealth Scholarship. L.G. is supported by BHF Award RM/l3/3/30159 and L.P.O. is funded by a Wellcome Trust Fellowship (grant no. 203568/Z/16/Z). N.F. was supported by BHF grant no. RG/13/14/30314. N.L.N. was supported by the Biotechnology and Biological Sciences Research Council (Institute Strategic Programmes BBS/E/B/000C0419 and BBS/E/B/000C0434). S.S. and M.R.B. were supported by the BHF Centre for Cardiovascular Research Excellence. Core support was provided by the Wellcome-MRC Cambridge Stem Cell Institute (grant no. 203151/Z/16/Z). The authors thank Osiris for providing the primary mesenchymal stem cells[47].

Author contributions

J.B. was the principal experimentalist and was responsible for study design and conceptualization, data acquisition and interpretation, production of figures and manuscript writing. L.P.O. performed tissue culture, 3D-EHT generation, force measurement and assisted during surgery. M.C. performed tissue culture and 3D-EHT generation. H.D. performed force measurement and RT–qPCR. P.H. was responsible for preparation of cell suspensions on the day of transplantation, necropsy, assisting during surgery and postoperative animal care. S.B. performed the casting of 3D-EHT and force measurement. L.G. performed tissue histology, immunofluorescence and sample preparation for RNAseq. N.L.N. performed the bioinformatics analysis. D.I. contributed conceptual ideas and critically revised the manuscript for important intellectual content. F.S. critically revised the manuscript for important intellectual content. F.W. performed the functional analysis of echocardiographs. A.B. performed the gene expression analysis. A.L. was responsible for experimental guidance and force measurement data analysis. W.G.B. was responsible for data interpretation and logistics. A.M. was responsible for animal surgery and logistics. N.F. was responsible for processing of histologic tissue and preparation of slides. M.R. was responsible for force measurement equipment. M.R.B. critically revised the manuscript for important intellectual content. C.E.M. was responsible for study design and conception, obtaining research funding, study supervision, and editing and final approval of the manuscript. S.S. was responsible for study design and conception, obtaining research funding, study supervision, interpretation of data, and editing and final approval of the manuscript.

Competing interests

A patent has been filed on the cardiac application of epicardial cells, on which C.E.M., S.S. and J.B. are coinventors (WO2018170280A1). C.E.M. is a scientific founder and equity holder in Cytocardia.

Additional information

Supplementary information is available for this paper at https://doi.org/10.1038/s41587-019-0197-9.

Reprints and permissions information is available at www.nature.com/reprints.

Correspondence and requests for materials should be addressed to C.E.M. or S.S.

Publisher's note: Springer Nature remains neutral with regard to jurisdictional claims in published maps and institutional affiliations.

Methods

Preparation of hESC-EPIs and hESC-derived CMs. Epicardial cells were differentiated from GFP-transgenic hESCs as previously described[12]. Briefly, hESCs (H9, WiCell) were maintained in a chemically defined medium (CDM-BSA) containing Activin-A (10 ng ml^{-1}, R&D Systems) and FGF2 (12 ng ml^{-1}, R&D Systems). Chemically defined medium consisted of IMDM (250 ml, Life Technologies), Ham's F12 (250 ml, Life Technologies), Pen/Strep (5 ml, Life Technologies), Insulin (350 µl, Roche), Transferrin (250 µl, Roche), chemically defined 100x lipid concentrate (5 ml, Life Technologies) and monothioglycerol (20 µl, Sigma). Differentiation to lateral mesoderm was performed as previously described in CDM-PVA, containing polyvinyl alcohol (PVA, 1 mg ml^{-1}, Sigma)[48]. In brief, early mesoderm differentiation was started with a combination of CDM-PVA, FGF2 (20 ng ml^{-1}), LY294002 (10 µM, Sigma) and BMP4 (10 ng ml^{-1}, R&D Systems) for 1.5 d. Then, lateral mesoderm differentiation was started in CDM-PVA, FGF2 (20 ng ml^{-1}) and BMP4 (50 ng ml^{-1}) for 3.5 d. To induce epicardial differentiation, cells were resuspended as single cells in CDM-PVA, WNT3A (25 ng ml^{-1}, R&D Systems), BMP4 (50 ng ml^{-1}) and retinoic acid (4 µM, Sigma) at a seeding density of 2.5×10^4 cm^{-2} for 10 d, and the medium was changed halfway through the differentiation. To generate epicardium-derived fibroblasts, epicardial cells were replated as single cells at a seeding density of 2.5×10^4 cm^{-2} and were grown under the influence of VEGF-B (50 ng ml^{-1}, Peprotech) and FGF2 (50 ng ml^{-1}) for 12 d. Flow cytometry was performed on day 10 epicardial cells using TCF21 (HPA013189, Atlas Antibodies) and WT1 (Ab89910, Abcam) antibodies on a BD FACS Calibur (BD Bioscience) and analyzed using FlowJo VX software version 9.9.4 (Fig. 1, panel b, and Supplementary Figs. 8 and 19).

For derivation of mesenchymal stem cells from hESCs, colonies were passaged, resuspended in CDM-PVA containing FGF2 (12 ng ml^{-1}) and SB431542 (10 µM) and seeded at a density of 30 colonies per cm^2 on gel-MEF-coated plates. Cells were enzymatically dispersed and passaged 4 times in CDM-PVA containing FGF and SB431542 before being split 1 more time in DMEM-F12 containing 10% fetal bovine serum for long-term maintenance. Primary mesenchymal stem cells (gift from Osiris) were also maintained in DMEM-F12 containing 10% fetal bovine serum.

CMs were generated from hESCs with the ABCX method as previously described[49,50]. In brief, hESCs (RUES2, female line, Rockefeller University, National Institutes of Health (NIH) registry number 0013) were maintained in feeder-free irradiated mouse embryonic fibroblast-conditioned medium containing bFGF (4 ng ml^{-1}, Peprotech). Cells were seeded as single cells (1×10^5 cm^{-2}) on matrigel (BD Biosciences)-coated plates with conditioned medium including Chiron 99021 (1 µM, Cayman Chemical) and ROCK inhibitor (Y-27632). The following day (day 0), the medium was aspirated and cells were fed with RPMI medium supplemented with B27 (Invitrogen) containing Activin-A (100 ng ml^{-1}) for 18 h. On day 1, medium was aspirated and cells were fed with RPMI medium plus B27 containing BMP4 (5 ng ml^{-1}) and Chiron 99021 (1 µM) for 48 h. On day 3, medium was aspirated and replaced with RPMI medium plus B27 containing Xav 939 (1 µM, Torcis). On day 5, the medium was replaced with RPMI medium plus B27. On day 7, the medium was replaced with RPMI containing B27 with insulin (Invitrogen) and was consequently replaced every other day until termination of the protocol.

CMs were frozen down on day 21 and the same batch was used for the entirety of the study. Flow cytometry was performed on thawed cells using cTnT antibody (Thermo, MS-295-P) on a BD FACSCanto II (Beckton Dickinson) and analyzed using FACSDiva software (BD Biosciences), revealing a purity of 97.1 ± 0.5% (cTnT$^+$, Fig. 1, panel b).

Epicardial cells were heat-shocked on the day before cell transplantation and CMs before freezing, both for 30 min at 42.5°C. On the day of cell transplantation, epicardial cells and CMs were enzymatically dispersed, counted and resuspended in 100 µl volume per rat of matrigel and prosurvival cocktail (PSC). PSC consisted of 50% (vol/vol) matrigel and ZVAD-FMK (100 µM, Calbiochem), Bcl-XL (50 nM, Calbiochem), Cyclosporin A (200 nM, Wako Pure Chemicals), Pinacidil (50 µM, Sigma) and IGF-1 (100 ng ml^{-1}, Peprotech). Cell preparations either contained matrigel plus PSC as vehicle controls, or 5×10^6 epicardial cells, 10×10^6 CMs or the combination of 5×10^6 epicardial cells and 10×10^6 CMs in matrigel/PSC.

Mycoplasma screening was performed on all cells on a regular basis and found to be negative.

Generation and functional assessment of 3D-EHT. To cast the tissue constructs, wells were fabricated using polydimethylsiloxane (PDMS) (Sylgard 184, Dow Corning). PDMS linker and base were mixed in a 1:10 mass ratio and poured in laser-etched acrylic negative templates featuring 4 wells measuring $3\times8\times2$ mm^3 and containing a 1-mm-diameter post positioned at 1.5 mm from each end. The PDMS was baked at 65 °C overnight, removed from the negatives and then autoclaved. Before casting the tissues, the PDMS wells were treated with 5% pluronic acid F127 solution (P2443, Sigma) for 1 h.

CMs used for construct studies were frozen down on day 21 of the differentiation and given 5 d in culture to recover. During construct casting, CMs and epicardial cells were trypsinized and mixed in a collagen gel containing 10x RPMI-1640 medium (Sigma), NaOH, geltrex (A1413202, Invitrogen), Collagen I Rat Protein (A1048301, Gibco Life Technologies) and water. The cell-gel solution was poured into the PDMS wells and allowed to solidify for 30 min at 37 °C. Each construct contained either 5×10^5 CMs alone or 5×10^5 CMs plus 5×10^4 supportive cells. Constructs were then fed with 7 ml RPMI medium plus B27 plus insulin every other day, and spontaneous contractions were observed within 7 d. All constructs were cultured for 14 d, fixed with 4% paraformaldehyde, treated with 30% sucrose at 4 °C overnight and finally cryoembedded and sectioned.

Myofibril alignment was quantified using an orientation correlation function (OCF) as previously described[51]: $\mathrm{OCF}=0.5\,(\cos(2\theta)+1)$, where θ is the difference between the angle of the myofibril fibril and the longitudinal CM axis.

For assessment of Ca^{2+} handling, 14-day-old constructs were incubated with fluo-4, AM (Molecular Probes, Invitrogen) for 20 min at 37 °C. Videos were taken with a Sony Handycam (Vixia HFS20) attached to a fluorescence microscope (Nikon Eclipse TS100). Videos were subsequently converted to frames, imported and analyzed using Image J software, normalizing the Ca^{2+} signal to baseline.

Force measurement of constructs was performed after 2 weeks in culture as previously described[52]. In brief, constructs were removed from the PDMS wells and suspended between a force transducer (model 400A, Aurora Scientific) and length controller (model 312B, Aurora Scientific). To assess the Frank–Starling relationship, constructs were stretched from their resting length to an additional 25% strain in 6 steps while being bathed in a HEPES-buffered Tyrode solution held at 37 °C. Force traces were first recorded without electrical stimulation and subsequently with 1, 1.5, 2 and 3 Hz at 5 V and 50 ms pulse duration. Passive tension and active force traces were recorded and analyzed using customized LabView and MATLAB software. A total of nine independent constructs were generated for each group and used for morphometric and functional analysis. The only exclusion criterion was tissue damage of the integrity of the loop regions. CMs were used from one frozen batch to ensure constant ultra-high purity and epicardial cells were used from three different differentiations.

Gene expression analysis. EHTs were dissociated and gene expression analyses performed after 2 weeks in culture. Total cellular RNA was extracted with ARCTURUS PicoPure RNA Isolation Kit (KIT0103, Applied Biosystems) with the following modifications. EHTs were placed in Lysing Matrix D beads (116913050, MP Biomedicals) and 200 µl Extraction Buffer and homogenized using a FastPrep-24 5G Instrument (MP Biomedicals). The resulting lysate was transferred to a fresh tube and incubated at 42 °C for 30 min. Then, 70% ethanol was added to the RNA lysate and loaded into a preconditioned column. All subsequent steps were performed according to the supplier's recommendations, including DNase I treatment. Next, 10 µl eluted RNA (corresponding to 100–150 ng) was subjected to reverse transcription using Maxima First Strand kit (K1641, Thermo) according to the manufacturer's protocol. RT–qPCR was performed with Fast SYBR Green Master Mix (4385610, Thermo) using 5 ng complementary DNA and 100 nM forward and reverse primers. Reactions were run on a 7900HT Fast Real-Time PCR System (4329001, Applied Biosystems), and data were analyzed using the ΔΔCt method using HPRT1 as the housekeeping gene. Primers were designed using PrimerBlast and confirmed to amplify a single product. A complete list is provided in Supplementary Table 3.

Injection of hPSC-derived epicardial cells in chicken embryos. Chicken (*Gallus gallus domesticus*) eggs (Winter Egg Farm) were incubated in a digital cabinet incubator (OVA Easy 380, Brinsea) at 38 °C. At Hamburger Hamilton developmental stage 19 (HH19), the eggshell was fenestrated, the window was covered with parafilm (VWR) and the eggs were placed horizontally in the incubator. At HH35, epicardial cells were transplanted in PSC with matrigel (1:2 dilution) onto the chorionic chicken vasculature. HESCs were fully differentiated to epicardial cells before administration into the chicken embryos. The eggs were then returned to the incubator until stage HH40. The matrigel plugs were collected and fixed in 4% paraformaldehyde before being stained with anti-HLA1 (Abcam), anti-SM22alpha (Abcam) and *Sambucus nigra* lectin (Vector Laboratories).

Myocardial infarction and cell transplantation. All studies were approved by the University of Washington Animal Care and Use Committee (protocol number 2225-04) and were conducted in accordance with US NIH Policy on Humane Care and Use of Laboratory Animals. The study design comprised two feasibility studies and one definitive study. The first study was designed to assess the acute survival and fate of hESC-EPIs. Animals either received 2×10^6 ($n=4$) or 4×10^6 ($n=4$) epicardial cells or a vehicle control injection ($n=4$). In a second feasibility study, designed to assess long-term survival of epicardial cells and their function, animals randomly received either 6×10^6 epicardial cells ($n=6$) or a vehicle control injection ($n=4$). The definitive study was conducted to assess the trophic effect of the epicardium on CMs. The definitive study design comprised the following 4 study arms: 5×10^6 epicardial cells ($n=15$), 10×10^6 CMs ($n=14$), 5×10^6 epicardial cells plus 10×10^6 CMs ($n=14$) and vehicle control ($n=13$). Animal deaths and cellular engraftment are presented in Supplementary Table 4.

The protocol for cell implantation has been previously detailed[8,34]. In brief, male athymic Sprague Dawley rats (Harlan/Envigo) underwent anesthesia through intraperitoneal injection of 68.2 mg kg^{-1} ketamine and 4.4 mg kg^{-1} xylazine, and were intubated and mechanically ventilated with room air and supplemented oxygen. A second dose of ketamine and xylazine was administered 20 min later. Animals were placed on a heating pad connected with a rectal temperature

probe, which ensured maintenance of body temperature at 37 °C. A thoracotomy was subsequently performed, the anterior surface of the heart was exposed and the left anterior descending coronary artery was visualized. The left anterior descending coronary artery was consequently ligated for 60 min after which the ligation was removed, the animal reperfused and the chest aseptically closed. At 4 d post-myocardial infarction, animals were anesthetized with isoflurane before undergoing a second thoracotomy for intramyocardial cell transplantations. Animals were subsequently randomly assigned to one of the treatment groups and cells were injected into the infarct zone. The chest was subsequently closed and the animals were postoperatively monitored.

To optimize graft retention, animals received daily subcutaneous injections of 5 mg kg^{-1} Cyclosporine A from the day before surgery until 7 d after the surgery. To assess cell proliferation in the cell grafts, animals were injected with 50 mg kg^{-1} BrdU on days 1, 4, 7 and 14 post-cell injection. The cohort of animals that was followed up for 3 months additionally received 1 BrdU injection 24 h before the termination of the study.

Echocardiography. All animals underwent echocardiographic exams at baseline before myocardial infarction, 4 d after the infarct and 28 d after cell transplantation. A subset of animals were maintained and imaged at 84 d post-transplantation. Briefly, animals were lightly anesthetized with inhaled isoflurane (Novaplus) and scanned by transthoracic echocardiography (GE Vivid 7) using a 10 S (10 MHz) pediatric probe. The end points acquired comprised fractional shortening (%), LVEDD and LVESD. LVDD and LVESD are expressed in millimeters. The images were anonymized and a primary reader made measurements in a blinded manner. For validation purposes an independent investigator analyzed a sample set of images in a blinded fashion before analysis of the entire data set and at the end to ensure consistency in measurements. The respective Bland–Altman plots and intraclass correlation coefficients of these two tests are presented in Supplementary Fig. 20. Details of histologic and echocardiographic parameters are presented in Supplementary Table 1.

Immunocytochemistry and immunohistochemistry. For immunocytochemistry, cells were fixed in 4% paraformaldehyde, permeabilized with 0.5% Triton X-100 in PBS and blocked in 3% BSA/PBS for 45 min at room temperature. Primary antibody incubations were performed at 4 °C overnight. The next day, cells were washed and incubated with Alexa-Fluor-conjugated secondary antibodies for 45 min at room temperature before staining with 4,6-diamidino-2-phenylindole (DAPI) for 10 min to visualize the nuclei. For immunohistochemistry, hearts were excised postmortem and prepared as described[34]. Briefly, hearts were washed in PBS, kept in saturated KCl for 20 min and subsequently fixed in 4% paraformaldehyde and paraffin sectioned (5 mm). For immunohistochemistry stainings, slides were deparafinized, underwent heat-mediated antigen retrieval for 15 min and were blocked with 5% BSA/PBS containing 0.3% Triton X-100 for 1 h at room temperature, followed by incubation with primary antibodies at 4 °C overnight, and fluorescent secondary antibodies were applied at room temperature for 60 min on the consecutive day. All antibodies used for immunocytochemistry and immunohistochemistry studies are detailed in Supplementary Table 5.

For quantification of sarcomeric length, a total number of 1,271 sarcomeres (129 CMs) were quantified in vitro (9 constructs) and 4,660 sarcomeres (407 CMs) were quantified in vivo (37 animals) by manual measurements in a blinded fashion.

Infarct and graft quantification. To assess infarct size, slides were stained with picrosirius red/fast-green stain. Subsequently, in the infarcted sections, picrosirius red-positive area was quantified and normalized to the left ventricular area in each section. For quantification of cardiac graft size, slides were stained overnight with human mitochondria antibody (Novus) and α-Actinin (Abcam) to quantify the size of the human cardiac grafts, followed by 1 h incubation with Alexa Fluor-488 donkey anti-rabbit and Alexa Fluor-568 goat anti-mouse secondary antibodies (Invitrogen). The corresponding graft size was then normalized to the size of the infarct area. All animals were used for analysis except one animal in the CM only study arm, which did not exhibit a detectable graft. Images were acquired on a Nikon TiE Inverted Widefield Fluorescence High-Resolution Microscope. To assess epicardial grafts, anti-GFP (Novus) and anti-human mitochondria (Novus) antibodies were used. For investigation of EMT of grafted epicardial cells, slides were stained with antibodies directed against GFP (Novus), vimentin (Dako) and wide-spectrum cytokeratin (Dako). To determine the fate of epicardial cells, slides were costained with antibodies directed against human mitochondria (Novus) and CMs (alpha-Actinin, Abcam), endothelial cells (human lectin (*Ulex europaeus*, Vector)), smooth muscle cells (Smooth Muscle α-Actin, Dako) or fibroblasts (S100A4, Abcam). To detect cardiac grafts, antibodies directed either against human mitochondria and α-Actinin or against β-MHC (Developmental Studies Hybridoma Bank) were used. For assessment of microvascular density, slides were stained with CD31/PECAM (Novus) and either β-MHC (Developmental Studies Hybridoma Bank) or cTnI (Abcam). For quantification of microvascular density in cardiac grafts, the infarct zone and the non-injured border zone, nine high-power images were taken in each of the three areas of interest. The number of lumens was counted and expressed as vessel number per area (mm^2). All images were acquired in technical replicates per animal on a Zeiss LSM700 microscope using ZEN software and were subsequently analyzed using ImageJ software. A detailed description of the antibodies and dilutions is provided in Supplemental Table 1.

RNA sequencing. The starting material for RNA sequencing was hESC-derived epicardium as used for all in vitro and in vivo experiments. For bulk RNA sequencing total RNA was extracted with the RNeasy Mini kit according to the manufacturer's instructions (Qiagen). This was followed by RNAse treatment to remove contaminating DNA. Samples were consecutively sent to the Genomics facility at the Wellcome Trust – Medical Research Council Cambridge Stem Cell Institute, where cDNA libraries were generated using the SMARTer Stranded Total RNA-Seq Kit.

All samples were sequenced on two lanes of an Illumina HiSeq2500. Short reads were mapped to the *Homo sapiens* genome GRCh38 using HISAT2 (ref. [53]). For each sample, the bam files corresponding to both lanes were merged with bamtools[54]. These data have been deposited in NCBI's Gene Expression Omnibus and are accessible through GEO Series accession number GSE122714 (ref. [55]).

The number of reads per sample varies from 10 million (NC1) to 24 million (NC2). Quality control and read count were performed with SeqMonk (https://www.bioinformatics.babraham.ac.uk/projects/seqmonk/). Differential expression analysis between differentiated epicardium and neural crest cells was performed with DESeq2 (ref. [56]). The list of 8,261 differentially expressed genes was filtered to retain: (1) only genes encoding putatively secreted proteins, according to the Human Protein Atlas (http://www.proteinatlas.org/humanproteome/secretome (ref. [53])); and (2) only genes annotated with the gene ontology term 'extracellular matrix organization' using QuckGO (https://www.ebi.ac.uk/QuickGO (ref. [57])). The heatmap only displays differentially expressed genes with an adjusted $P < 1 \times 10^{-7}$, and was performed using the function heatplot of the package made4 on the $\log_2$ of reads per million reads values[58]. For clustering, heatplot uses Pearson correlation distances and the average agglomeration method. The gene ontology enrichment was performed with WebGestalt[59]. A complete list of the genes and their expression is shown in Supplementary Table 2.

Statistics. All in vitro studies were performed with three biological replicates (independent experiments performed on different days), each of which was performed using three technical replicates. All in vivo data specifically state the number of animals assessed for each time point. The normal distribution of our values was confirmed using the D'Agostino and Pearson omnibus normality test where appropriate. Variance between samples was tested with the Brown–Forsythe test. Statistical testing was performed using an unpaired *t*-test for two-group comparisons and a paired *t*-test for comparison of two paired groups. For multiple-group comparison a one-way ANOVA with a post-hoc Tukey test was used if the group variance was equal, and a Kruskall–Wallis test with Dunn's correction for multiple comparisons was applied for groups with unequal variance. Measuring two-sided significance, a *P* value of 0.05 was considered statistically significant. All analyses were performed using GraphPad Prism software in a blinded fashion. All results are expressed as mean ± s.d., unless otherwise stated.

For all in vivo experiments, group sizes were estimated based on power analyses using previous study variance. While no formal methods of randomization were used, the animals were randomly selected by a technician who was blinded to treatment. Analysis of all histology slides as well of all functional data was done in a blinded fashion. Death was the only exclusion criteria for further histologic and functional analysis. Supplementary Table 4 details animal mortality and grafting.

Reporting Summary. Further information on research design is available in the Nature Research Reporting Summary linked to this article.

Data availability

The raw data that support the findings of this study are available from the corresponding author upon reasonable request.

References

48. Bargehr, J. et al. Embryological origin of human smooth muscle cells influences their ability to support endothelial network formation. *Stem Cells Transl. Med.* **5**, 946–959 (2016).
49. Hofsteen, P., Robitaille, A. M., Chapman, D. P., Moon, R. T. & Murry, C. E. Quantitative proteomics identify DAB2 as a cardiac developmental regulator that inhibits WNT/beta-catenin signaling. *Proc. Natl Acad. Sci. USA* **113**, 1002–1007 (2016).
50. Palpant, N. J., Hofsteen, P., Pabon, L., Reinecke, H. & Murry, C. E. Cardiac development in zebrafish and human embryonic stem cells is inhibited by exposure to tobacco cigarettes and e-cigarettes. *PloS ONE* **10**, e0126259 (2015).
51. Young, J. L. & Engler, A. J. Hydrogels with time-dependent material properties enhance cardiomyocyte differentiation in vitro. *Biomaterials* **32**, 1002–1009 (2011).

52. Ruan, J. L. et al. Mechanical stress promotes maturation of human myocardium from pluripotent stem cell-derived progenitors. *Stem Cells* **33**, 2148–2157 (2015).
53. Kim, D., Langmead, B. & Salzberg, S. L. HISAT: a fast spliced aligner with low memory requirements. *Nat. Methods* **12**, 357–360 (2015).
54. Barnett, D. W., Garrison, E. K., Quinlan, A. R., Stromberg, M. P. & Marth, G. T. BamTools: a C++ API and toolkit for analyzing and managing BAM files. *Bioinformatics* **27**, 1691–1692 (2011).
55. Edgar, R., Domrachev, M. & Lash, A. E. Gene Expression Omnibus: NCBI gene expression and hybridization array data repository. *Nucleic Acids Res.* **30**, 207–210 (2002).
56. Love, M. I., Huber, W. & Anders, S. Moderated estimation of fold change and dispersion for RNA-seq data with DESeq2. *Genome Biol.* **15**, 550 (2014).
57. Binns, D. et al. QuickGO: a web-based tool for Gene Ontology searching. *Bioinformatics* **25**, 3045–3046 (2009).
58. Eisen, M. B., Spellman, P. T., Brown, P. O. & Botstein, D. Cluster analysis and display of genome-wide expression patterns. *Proc. Natl Acad. Sci. USA* **95**, 14863–14868 (1998).
59. Wang, J., Vasaikar, S., Shi, Z., Greer, M. & Zhang, B. WebGestalt 2017: a more comprehensive, powerful, flexible and interactive gene set enrichment analysis toolkit. *Nucleic Acids Res.* **45**, W130–W137 (2017).

nature research

Corresponding author(s): Sanjay Sinha

Last updated by author(s): 28/05/2019

Reporting Summary

Nature Research wishes to improve the reproducibility of the work that we publish. This form provides structure for consistency and transparency in reporting. For further information on Nature Research policies, see Authors & Referees and the Editorial Policy Checklist.

Statistics

For all statistical analyses, confirm that the following items are present in the figure legend, table legend, main text, or Methods section.

n/a	Confirmed	
☐	☒	The exact sample size (*n*) for each experimental group/condition, given as a discrete number and unit of measurement
☐	☒	A statement on whether measurements were taken from distinct samples or whether the same sample was measured repeatedly
☐	☒	The statistical test(s) used AND whether they are one- or two-sided *Only common tests should be described solely by name; describe more complex techniques in the Methods section.*
☐	☒	A description of all covariates tested
☐	☒	A description of any assumptions or corrections, such as tests of normality and adjustment for multiple comparisons
☐	☒	A full description of the statistical parameters including central tendency (e.g. means) or other basic estimates (e.g. regression coefficient) AND variation (e.g. standard deviation) or associated estimates of uncertainty (e.g. confidence intervals)
☐	☒	For null hypothesis testing, the test statistic (e.g. *F*, *t*, *r*) with confidence intervals, effect sizes, degrees of freedom and *P* value noted *Give P values as exact values whenever suitable.*
☒	☐	For Bayesian analysis, information on the choice of priors and Markov chain Monte Carlo settings
☒	☐	For hierarchical and complex designs, identification of the appropriate level for tests and full reporting of outcomes
☐	☒	Estimates of effect sizes (e.g. Cohen's *d*, Pearson's *r*), indicating how they were calculated

Our web collection on statistics for biologists contains articles on many of the points above.

Software and code

Policy information about availability of computer code

Data collection	No software was used for data collection in this study.
Data analysis	All statistical analysis was performed using GraphPad Prism software in a blinded fashion. Specific software used for individual experiments are detailed in the methods section of the manuscript. Images were acquired Images were acquired on a Zeiss LSM700 using ZEN software (Carl Zeiss AG, Jena, Germany). Image analysis was performed with Image J version 1.52k. Flow cytometric analysis was performed with FlowJo VX software version 9.9.4. Force generation of 3D-EHTs was analysed with Matlab R2015b (Mathworks) and LabView 2012 SP1 (National Instruments).

For manuscripts utilizing custom algorithms or software that are central to the research but not yet described in published literature, software must be made available to editors/reviewers. We strongly encourage code deposition in a community repository (e.g. GitHub). See the Nature Research guidelines for submitting code & software for further information.

Data

Policy information about availability of data

All manuscripts must include a data availability statement. This statement should provide the following information, where applicable:

- Accession codes, unique identifiers, or web links for publicly available datasets
- A list of figures that have associated raw data
- A description of any restrictions on data availability

The full RNA sequencing has been deposited in NCBI's Gene Expression Omnibus and are accessible through GEO Series accession number GSE122714 (https://www.ncbi.nlm.nih.gov/geo/query/acc.cgi?acc=GSE122714). The data that support the findings of this study are available from the corresponding author upon reasonable request.

Field-specific reporting

Please select the one below that is the best fit for your research. If you are not sure, read the appropriate sections before making your selection.

☒ Life sciences ☐ Behavioural & social sciences ☐ Ecological, evolutionary & environmental sciences

For a reference copy of the document with all sections, see nature.com/documents/nr-reporting-summary-flat.pdf

Life sciences study design

All studies must disclose on these points even when the disclosure is negative.

Sample size	Sample size has not been formally predetermined but was based on previous studies from the Murry group.
Data exclusions	The only exclusion criterion for in vitro analysis of 3D-EHTs was tissue damage of the integrity of the loop regions as this would have confounded functional and structural measurements of the construct. The only exclusion criterion for animals in vivo was death following myocardial infarction or cell transplantation.
Replication	In vitro N=9 constructs per experimental group were generated independently and measured on three different days. In vivo N=60 athymic rats were used for the main study. Numbers of constructs and animals used in each individual experiment are detailed in the figure legends. All attempts of replication were successful.
Randomization	While no formal methods of randomization were used, the animals were randomly selected by a technician who was blinded to treatment.
Blinding	All investigators involved during data collection and analysis were blinded to treatment goup and group allocation.

Reporting for specific materials, systems and methods

We require information from authors about some types of materials, experimental systems and methods used in many studies. Here, indicate whether each material, system or method listed is relevant to your study. If you are not sure if a list item applies to your research, read the appropriate section before selecting a response.

Materials & experimental systems

n/a	Involved in the study
☐	☒ Antibodies
☐	☒ Eukaryotic cell lines
☒	☐ Palaeontology
☐	☒ Animals and other organisms
☒	☐ Human research participants
☒	☐ Clinical data

Methods

n/a	Involved in the study
☒	☐ ChIP-seq
☐	☒ Flow cytometry
☒	☐ MRI-based neuroimaging

Antibodies

Antibodies used

All antibodies used are listed in supplementary table 5 as follows
(Antibody; Application; Species; Dilution; Manufacturer (Cat#)):

Vimentin, Clone Vim 3B4; ICC/IHC; Mouse; 1:100; Dako (M7020)
Cytokeratin; ICC/IHC; Rabbit; 1:150; Dako (Z0622)
GFP; IHC; Goat; 1:500; Novus (NB-100-1770)
Human Mitochondria, Clone 113-1; IHC; Mouse; 1:100; Millipore (MAB1273)
Fibronectin; IHC; Rabbit; 1:250; Abcam (ab2413)
Alpha-Actinin; IHC; Rabbit; 1:800; Abcam (ab68167)
Cardiac Troponin I; IHC; Rabbit; 1:200; Abcam (ab47003)
Cardiac Troponin T; IHC; Goat; 1:200; Abcam (ab64623)
Cardiac Troponin T; IHC; Mouse; 1:200; Abcam (ab8295)
Connexin 43; IHC; Mouse; 1:500; Millipore (MAB3067)
Connexin 43; IHC; Rabbit; 1:500; Abcam (ab11370)
Beta-Myosin Heavy Chain, Clone A4.951; IHC; Mouse; Full strength; Human Hybridoma Bank
CD31/ PECAM-1; IHC; Rabbit; 1:100; Novus (NB100-2284)
Biotinylated human Lectin; IHC; Ulex europaeus; 1:1000; Vector (B-1065)
S100A4 ICC; IHC; Rabbit; 1:100; Abcam (ab124805)
DDR2; ICC; Goat; 1:50; Santa Cruz (sc-7555)
Smooth Muscle Alpha Actin; IHC; Mouse; 1:200; Dako (M0851)
Smooth Muscle Alpha Actin; IHC; Goat; 1:200; Abcam (ab21027)
Anti-BrdU-POD, Clone BMG-6H8; IHC; Mouse; 1:40; Roche (11 585 860 001)

SM-22; IHC; Rabbit; 1:400; Abcam (ab14106)
cTnT; Flow; Mouse; 1:100; Thermo Fisher (MS-295-P)
TCF21; Flow; Rabbit; 1:250; Atlas Antibodies (HPA013189)
WT1; Flow; Rabbit; 1:500; Abcam (Ab89910)
Alexa Fluor 647; Flow; Chicken anti Rabbit IgG; 1:200; Invitrogen (A21443)
Alexa Fluor 488; IHC; Rabbit anti Mouse IgG; 1:100; Invitrogen (A11054)
Alexa Fluor 488; IHC; Goat anti Mouse IgG; 1:100; Invitrogen (A11001)
Alexa Fluor 488; IHC; Donkey anti mouse IgG; 1:100; Invitrogen (A21202)
Alexa Fluor 488; IHC; Donkey anti Goat IgG; 1:100; Invitrogen (A11055)
Alexa Fluor 488; IHC; Donkey anti rabbit IgG; 1:100; Invitrogen (A21206)
Alexa Fluor 488; IHC; Rabbit anti goat IgG; 1:100; Invitrogen (A11078)
Alexa Fluor 488; IHC; Goat anti rabbit IgG; 1:100; Invitrogen (A110034)
Alexa Fluor 568; IHC; Goat anti mouse IgG; 1:100; Invitrogen (A11031)
Alexa Fluor 568; IHC; Donkey anti mouse IgG; 1:100; Invitrogen (A10037)
Alexa Fluor 568; IHC; Rabbit anti mouse IgG; 1:100; Invitrogen (A11061)
Alexa Fluor 568; IHC; Donkey anti rabbit IgG; 1:100; Invitrogen (A10042)
Alexa Fluor 568; IHC; Donkey anti Goat IgG; 1:100; Invitrogen (AA21432)
Alexa Fluor 647; IHC; Donkey anti mouse IgG; 1:100; Invitrogen (A31571)
Alexa Fluor 647; IHC; Donkey anti goat IgG; 1:100; Invitrogen (A21447)
Alexa Fluor 647; IHC; Goat anti rabbit IgG; 1:100; Invitrogen (A21244)

Validation

The validity of each antibody was tested using positive and negative controls using 4% PFA fixed and paraffin embedded rat heart sections or 4% PFA fixed and paraffin embedded human fetal hearts. Control stainings are displayed in the figures.

Eukaryotic cell lines

Policy information about cell lines

Cell line source(s)

hESCs (RUES2, Female line, Rockefeller University) & hESCs (H9, WiCell, Madison)

Authentication

Cell lines were obtained directly from the provider. No formal form of authentication was carried out.

Mycoplasma contamination

Mycoplasma screening was performed on the cell lines and was negative.

Commonly misidentified lines
(See ICLAC register)

None of the cell lines used in this study are listed in the ICLAC database.

Animals and other organisms

Policy information about studies involving animals; ARRIVE guidelines recommended for reporting animal research

Laboratory animals

Male athymic Sprague Daley rats (Harlan/Envigo); age: 8-10 weeks on arrival.

Wild animals

This study did not use wild animals.

Field-collected samples

The study did not involve samples collected from the field.

Ethics oversight

All studies were approved by the University of Washington Animal Care and Use Committee (IACUC; protocol number 2225-04) and were conducted in accordance with US NIH Policy on Humane Care and Use of Laboratory Animals.

Note that full information on the approval of the study protocol must also be provided in the manuscript.

Flow Cytometry

Plots

Confirm that:

☒ The axis labels state the marker and fluorochrome used (e.g. CD4-FITC).

☒ The axis scales are clearly visible. Include numbers along axes only for bottom left plot of group (a 'group' is an analysis of identical markers).

☒ All plots are contour plots with outliers or pseudocolor plots.

☒ A numerical value for number of cells or percentage (with statistics) is provided.

Methodology

Sample preparation

Cardiomyocytes were frozen down on day 21, thawed and then used for experiments, including flow cytometry, using a standard protocol and primary antibodies as follows: TCF21 (Atlas antibodies, HPA013189), WT1 (Abcam, Ab89910) and cTnT antibody (Thermo, MS-295-P).

Instrument	Data were collected using: 1) BD FACS Calibur (BD Bioscience) for hESC-epicardial cells and 2) BD FACSCanto II (Beckton Dickinson, San Jose, CA) for hESC-cardiomyocytes.
Software	Flow cytometric analysis was performed with FlowJo VX software version 9.9.4.
Cell population abundance	Flow cytometry revealed a purity of 97.1% for hESC-derived cardiomyocytes and a purity of 73.2% for epicaridal cells (Figure 1, panel b).
Gating strategy	HESC-derived cardiomyocytes and hESC-derived epicardial cells were used as a starting population. Cells were gated on FSC/SSC first and an unstained sample, IgG isotype and secondary only as controls to establish the gate for positive cells.

☒ Tick this box to confirm that a figure exemplifying the gating strategy is provided in the Supplementary Information.